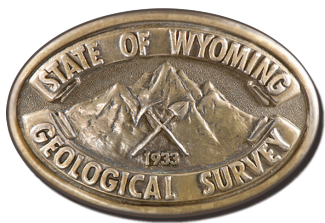


Interpreting the past, providing for the future

Preliminary Geologic Map of the Albany 7.5' Quadrangle, Albany County, Wyoming

By Wayne M. Sutherland and Natali A. Kragh

Open File Report 2018-1
April 2018



Wyoming State Geological Survey

Erin A. Campbell, Director and State Geologist



Preliminary Geologic Map of the Albany 7.5' Quadrangle, Albany County, Wyoming

By Wayne M. Sutherland and Natali A. Kragh

Layout by Christina D. George

Open File Report 2018-1
Wyoming State Geological Survey
Laramie, Wyoming: 2018

This Wyoming State Geological Survey (WSGS) Open File Report is preliminary and may require additional compilation and analysis. Additional data and review may be provided in subsequent years. For more information about the WSGS, or to download a copy of this Open File Report, visit www.wsgs.wyo.gov. The WSGS welcomes any comments and suggestions on this research. Please contact the WSGS at 307-766-2286, or email wsgs-info@wyo.gov.

Citation: Sutherland, W.M., and Kragh, N.A., 2018, Preliminary geologic map of the Albany quadrangle, Albany County, Wyoming: Wyoming State Geological Survey Open File Report 2018-1, 45 p., 1 pl., scale 1:24,000.

Table of Contents

Introduction	1
Samples	2
Mineralization	3
Florence Trend	4
Cuprite Trend.	4
Mammoth trend.	6
Vesuvius trend	7
Other prospects	8
Lake Creek district	8
Lake Owen mafic complex.	8
Browns Park Formation	9
REE	9
Critical and Strategic Elements.	9
Description of Map Units	9
References	23
Appendices	27
Appendix 1: Sample descriptions and locations	28
Appendix 2: Whole rock chemical analyses.	30
Appendix 3: Albany quadrangle Trace element chemical analyses.	31
Appendix 4: Radiometric dating of samples from within the Albany quadrangle	35

List of Figures

Figure 1. Red rectangle is the approximate location of the Albany quadrangle.	1
Figure 2. Historic log-lined, collapsed shaft along the Cuprite trend.. . . .	5
Figure 3. Collapsed adit southeast of the Endymion lode.	7
Figure 4. Collapsed shaft and shaft house at the Vesuvius lode.	7
Figure 5. Limestone with felsic breccia in the Browns Park Formation.	11
Figure 6. Brecciated limestone tufa in the Browns Park Formation.	11
Figure 7. Agate and opal pieces characteristic of the White River Formation	12
Figure 8. Pegmatite with chilled margins and alternating layers of fine and coarse crystals.	14
Figure 9. Luxullianite with black schorl crystals.	16
Figure 10. Typical broken surface of mylonitic gneiss.	17

Figure 11. Gabbro-norite within the Lake Owen layered unit showing changes in crystal sizes.	18
Figure 12. Lake Owen border phase gneiss with xenoliths.	19
Figure 13. Medium- to coarse-grained Horse Creek foliated granodiorite with mafic xenolith at top.	19
Figure 14. Typical foliation within the Horse Creek foliated granodiorite.	19
Figure 15. Typical freshly exposed Keystone Quartz Diorite.	20
Figure 16. One of many variabilities within the Keystone Quartz Diorite transition zone.	21
Figure 17. Finely layered contorted gneiss.	22

INTRODUCTION

The Albany quadrangle is one of several quadrangles, not previously mapped in detail, that cover a portion of the Southern Medicine Bow Mountains Mining District. In addition to detailed mapping, this project focuses on determining the petrologic and structural geologic history that influenced mineralization of Au, Ag, Cu, platinum-group elements (PGE), V, Ti, Fe, and rare earth elements (REE). This map presents a revision of several previous investigations in the area. The map was completed in cooperation with the U.S. Geological Survey (USGS) 2017 STATEMAP grant award #G17AC00117 to the Wyoming State Geological Survey (WSGS).

Mapping was conducted through on-the-ground examination and measurement of rock units, aerial imagery interpretation, and compilation of previous mapping and written reports. Initial mapping of the quadrangle in 2004 began with aerial photographic interpretation and compilation of a wide variety of source material by Wayne M. Sutherland and W. Dan Hausel, which was incorporated into the 1:100,000-scale Saratoga 30' x 60' quadrangle (Sutherland and Hausel, 2005a). Field work by the authors, conducted from June through September 2017, included attitude measurements along with identification and sampling of various rock units, structural features, and mineralized areas. Photos in this report are by Wayne M. Sutherland and Natali A. Kragh.

We wish to thank Malcolm E. McCallum for access to unpublished mapping by him and Robert S. Houston that was compiled in 1985, which significantly influenced our 2017 mapping efforts. Our thanks also to Dr. Kevin R. Chamberlain for helping us to understand the local geochronology and for his geochronologic evaluation of our samples.

LOCATION AND GEOLOGIC SETTING

The quadrangle lies in southeastern Wyoming in the Medicine Bow Mountains, a Laramide uplift that exposes Archean Wyoming Craton in the north and the Paleoproterozoic Colorado Province in the south (fig. 1). The boundary between the two provinces is a collision zone marked by the Cheyenne belt, a 1,780–1,740 Ma suture characterized by synmetamorphic rocks and subvertical shear zones (Houston, 1993; Sullivan and Beane, 2013). The quadrangle lies on the southern edge of the Cheyenne belt, within a zone of volcanogenic island-arc basement rocks, supracrustal rocks, and intrusive granitic rocks (Houston and others, 1968; Graff, 1978; Hills and Houston, 1979; Houston, 1993). Extensive shearing crosses much of the quadrangle, with northeast trends near the northern edge, east to southeast trends in the central part, and east to northeast trends near the southern edge.

Rocks in the map area comprise predominantly Proterozoic-age crystalline rocks with limited Phanerozoic rocks. Multiple deformational events have resulted in both ductile and brittle geologic structures. Along the northeast edge of the map, Laramide faults juxtapose Precambrian basement against Paleozoic and Mesozoic sedimentary rocks. At high elevations across the quadrangle, the Miocene-

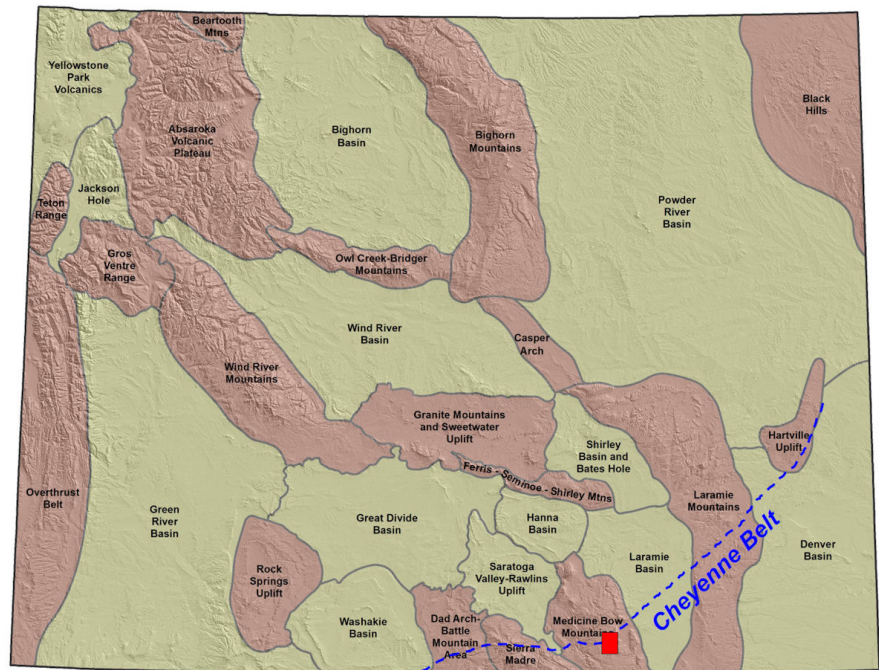


Figure 1. Red rectangle is the approximate location of the Albany quadrangle.

Oligocene Browns Park and the Oligocene–Eocene White River formations remain as erosional remnants from post-Laramide, pre-Miocene-uplift and basin fill.

Small exposures of the $1,777.6 \pm 2.1$ Ma (Snyder, 1980) Mullen Creek layered mafic complex occur only in the northwestern corner of the quadrangle within part of the Rambler Splay of the Mullen Creek–Nash Fork Shear Zone; the majority of the complex is west of the Albany quadrangle. The Rambler Splay is a broad area of east- to northeast-trending shearing and mylonites that includes the northwestern corner of the quadrangle, much of which is covered by Tertiary and Quaternary deposits. Outcrops of the 1775.1 ± 3.0 Ma Lake Owen layered mafic complex comprise most of the southeastern quarter of the Albany quadrangle.

Surrounding the mafic complexes are gneisses and schists interpreted to have metavolcanic and metasedimentary origins (Houston and others, 1968; Houston, 1993). Igneous intrusions include the older 1784.7 ± 1.9 Ma Keystone Quartz Diorite, the younger $1,770.8 \pm 3.4$ Rambler Granite (Premo and Loucks, 2000), and the $1,433 \pm 1.5$ Ma Sherman Granite (Frost and others, 1999). Both felsic and mafic Mesoproterozoic dikes of undetermined ages intrude at least some of the previously mentioned rock types.

The diversity of igneous events and structural activity in the map area has created complex interrelationships that are difficult to interpret.

SAMPLES

A total of 141 samples were collected, of which 24 were chosen for thin sections, 31 for geochemical analyses by an outside commercial laboratory, and 3 for radiometric dates.

Samples collected for geochemical analyses are grab samples, which generally do not represent a large or measured volume of material greater than that of the sample itself. Elemental concentrations associated with a grab sample may or may not extend into the outcrop from which the sample was collected. Analyses of these samples can neither confirm nor deny the presence or absence of economic concentrations of various elements.

Thin sections were prepared by Wagner Petrographics of Lindon, Utah. Observations from thin sections are included within map unit descriptions where appropriate. Radiometric dating was conducted under the direction of Dr. Kevin R. Chamberlain, Department of Geology and Geophysics, University of Wyoming. Geochemical analyses, including whole rock chemistry, trace elements, REE, and gold were completed by ALS Chemex of Reno, Nevada. Geochemical analyses on samples included whole rock analyses (major element concentrations in the form of oxides) by inductively coupled plasma, atomic emission spectrometry or mass spectrometry, and atomic adsorption.

Most samples were analyzed with in-house X-ray fluorescence using an Olympus Vanta M series handheld X-ray fluorometer. When discussed in the text, this type of analysis is referred to as “WY-XRF” to separate it from analytical results from an outside commercial laboratory. WY-XRF results often include multiple measurements of heterogeneous samples. “ $\leq\#$ ” value indicates a composite of the highest parts per million (ppm) measurements in several circular focus areas about 4.5 mm across, which may not be representative of the entire sample.

Prior to this mapping effort, several samples were collected and analyzed in conjunction with a statewide survey of potential sources of REE (Sutherland and others, 2013; Sutherland and Cola, 2016). Sample results from these projects and the current investigation, including descriptions, photographs, and analyses, are available upon request. Appendix 1 lists samples and their descriptions, and appendix 2 lists whole rock analyses for samples collected within the Albany quadrangle during this project. Appendix 3 lists trace elements for these samples. Appendix 4 provides details for radiometric dating of samples from within the Albany quadrangle.

MINERALIZATION

The Southern Medicine Bow Mountains Mining District is defined to include all mines, prospects, and mineralized areas in the Medicine Bow Mountains south of, and including, the Cheyenne belt. As such, the district encompasses several historic mining districts. The Albany quadrangle incorporates a portion of the Keystone mining district (all mineralized trends and scattered prospects along the western edge of the quadrangle), where Au and Cu are concentrated along faults and shear zones related to the Cheyenne belt (Currey, 1965; Loucks, 1976; Hausel, 1989; 1997). Part of the Lake Creek mining district encroaches on the southwestern corner of the quadrangle. The Albany quadrangle also includes gold placer deposits along several creeks and minor anomalous concentrations of critical and strategic elements (CSEs) and REE (>5x average crustal abundance) in a variety of rock types. The Paleoproterozoic Lake Owen layered mafic complex in the southeastern part of the quadrangle hosts PGE-Au-V-Ti-Fe mineralization (Loucks, 1976).

Many of the rocks within the quadrangle have undergone metasomatic alteration. The related influx of hot fluids along faults and shear zones created erratic pods of precious and base metals that attracted miners beginning in the 1860s. Currey (1965) notes that copper and gold deposits concentrated over a relatively narrow vertical range. Better Cu grades occur in the supergene lower part of the oxidized zone, while free-milling gold concentrated in well-oxidized hypogene gold-bearing sulfides. Currey (1965) also notes increased potash content in sheared versus unsheared quartz diorite in the Lake Creek district. However, analyses (both external and WY-XRF) of 2017 samples in general show the opposite relationship with unsheared Sherman Granite, Keystone Quartz Diorite, felsic dikes, and some pegmatites hosting significantly more K₂O than found in sheared samples.

Epidote is commonly associated with metal occurrences within the quadrangle, regardless of adjacent rock types. It is also common at contacts and transition zones between various rock types, along felsic dikes and quartz veins, and along faults and shear zones. Strickland (2004) suggests that syndeformational epidote and sphene developed at ca. 1.60 Ga during northwest-directed, subhorizontal shortening during a previously unrecognized tectonic event. Radiometric dating was attempted on epidote samples that were closely associated with mineralization. However, results were inconsistent, suggesting that there is a wide range in the age of epidote formation, and mineralization may be related to both magmatic and metamorphic events.

McCallum and Houston (1985) note that all vein deposits examined in the Albany quadrangle appeared to be associated with mafic rocks within faults or shear zones, regardless of the composition of adjacent host rocks. Field examinations of numerous inactive mines and prospects, as part of the current study, seem to confirm this conclusion. Precious and base metal values probably derived from leaching of sheared and pulverized mafic rocks by fluids introduced along faults and shear zones with accompanying redeposition in lower pressure dilatant zones (Currey, 1965; McCallum and Orback 1968). Most mineralization occurs along southeast-trending faults and shears, especially at cross-fault intersections, along subsidiary fault splays or tear faults, and in the vicinity of cymoid flexures in faults (McCallum and Houston, 1985). East-trending faults in the west-central part of the quadrangle (Monarch trend) and east-trending shear zones in the southern part of the quadrangle also host some mineralization (Currey, 1965). Silicified rock, small irregular quartz-carbonate veins, and epidotization accompany most historic mines and prospects (Hausel, 1989). Calcite/ankerite veins, varying from 1 mm (0.04 in) to greater than 20 cm (8 in), accompany a majority of mines and prospects visited in 2017. Contact interactions between various igneous intrusions may also have influenced primary mineralization.

MINES AND MINERALIZED TRENDS

The Albany 7.5' quadrangle hosts several historic mines for both gold and copper dating from the mid- to late-1800s into the 1900s (Hausel, 1989; 1997). Some of these small mines operated intermittently through the mid-1900s, but records of significant production are not known. Historic mines slowly closed over time as rich pods along major trends were exhausted or became casualties of politics, low metals prices, or a lack of technology. No commercial mines are currently operating within the Albany quadrangle.

Gold was first discovered in the Medicine Bow Mountains in placers at Moore's Gulch in 1868 (Beeler, 1906; Currey, 1965) near the western edge of the Albany quadrangle. Placer activity included the lower reaches of Willow and Lewis creeks, which have headwaters near the western edge of the Albany quadrangle, Douglas Creek, which cuts the far southwestern corner of the quadrangle, and stretches of Muddy and Spring creeks in the southwestern part of the quadrangle (McCallum and Houston, 1985). Intermittent placer operations continued into the 20th century. The amount of historical production from within the Albany quadrangle is unknown. Current placer interests include Spring, Jim, Muddy, and Douglas creeks; most placer operations since the 1990s have typically been small-scale, hobby-type operations.

Little, if any modern exploration, such as drilling or geophysics, has been directed toward the metals deposits in the Medicine Bow Mountains. The only known exception is platinum exploration, which targeted both the Lake Owen and Mullen Creek complexes in the late 1900s and early 2000s. Claim staking for gold and for diamonds occurred in early summer 2017 within the Albany quadrangle.

Mineralized trends are generalized linear occurrences of metal mineralization that were historically named for one or more prominent mines along the trend. These trends relate to a variety of factors including faults, shears, dikes, veins, and alteration zones. Historical usage requires description of these trends and their depiction on the Albany quadrangle.

Florence Trend

The Florence mine, just off of the western edge of the Albany quadrangle (SE¼ sec. 22, T. 14 N., R. 79 W., along Jim Creek) is on the Keystone-Florence fault, about 1.2 km (0.75 mi) southeast of the Keystone mine. Developments related to the Florence mine extend into the Albany quadrangle. Mineralization on or near this southeast-trending fault is referred to as the Florence trend, which cuts Keystone Quartz Diorite within the Albany quadrangle and extends into quartz-biotite gneiss (schist) to the northwest in the Keystone quadrangle. The width of the Florence trend is variable and locally exceeds 213 m (700 ft) near the Florence mine where it includes parallel faults and veins. The Keystone mine, to the west in the Keystone quadrangle, was one of the premier Cu-Au mining operations in the early 1890s. Production at the Florence mine was entirely Au from auriferous pyrrhotite in quartz-ankerite veins (McCallum and Houston, 1985).

The Florence mine developed a 0.9–1.5 m (3–5 ft) wide ore shoot with an approximately 50-m (160-ft) shaft accompanied by 37 m (120 ft) of drifts and stopes on the 9-m (30-ft) level and shorter drifts on the 30-m (100-ft) level before the mine closed in 1889 (Anonymous, 1896; Knight, 1942; Currey, 1965). Gold, valued at \$50,000, was reportedly recovered from discontinuous and irregular auriferous pyrrhotite kidneys in quartz-ankerite veins (McCallum and Houston, 1985) that yielded from \$155 to \$1,000 per ton in 1890 prices (Anonymous, 1896; Currey, 1965). Most of the gold was finely divided and not free-milling (Beeler, 1906), but was considered to be suited to cyanide or chlorination treatment (Currey, 1965).

Several efforts to reopen the Florence mine, as recently as the 1970s, were unsuccessful. USGS assays of seven samples of sulfide and limonite collected from the mine dump ranged from 0.1–30 ppm Ag, 2.0–800 ppm Au, 15–700 ppm Co, and 0.003–0.2 percent Cu (McCallum and Houston, 1985).

Numerous prospects and at least one shaft puncture the Florence trend southeast of the Florence mine. Only minor mineralization was noted in any of these. Sample 20170825NK-A from an adit and shaft in the Keystone Quartz Diorite showed 0.02 ppm Au. WY-XRF of several samples along this trend show ≤ 6 ppm Ag, ≤ 0.56 percent Cu, ≤ 173 ppm La, and ≤ 109 ppm Ta.

Cuprite Trend

The Cuprite mineralized trend follows the southeast- to east-trending Albany-Cuprite fault. Although the fault crosses most of the quadrangle and prospects are found near the town of Albany in the eastern part of the quadrangle,

gle, the term Cuprite trend generally refers to the western area of mineralization. Several adits, shafts (fig. 2), and prospect pits are located along this trend. The Cuprite adit cuts into a very fine-grained mafic dike with abundant potassium feldspar, epidote, and small quartz veins, which are all crosscut by massive calcite veins and surrounded by the Horse Creek foliated granodiorite.

The Cuprite mine, just south of Moores Gulch near the central western edge of the quadrangle (NW ¼ sec. 11, T. 14 N., R. 79 W.) was discovered in 1900. It is about 1.2 km (0.75 mi) southeast of the Albany mine in the Keystone quadrangle and about 0.6 km (0.4 mi) west of the Bear mine. The Albany mine primarily produced from low-grade Cu ores (Currey, 1965), but Au values of as much 20 ppm were obtained from samples by McCallum and Houston (1985). Loucks (1976) recognized electrum in vein quartz.

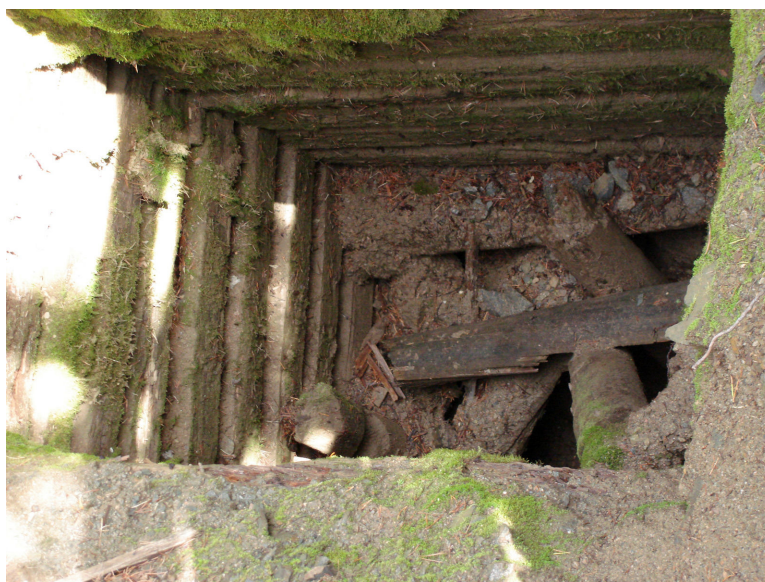


Figure 2. Historic log-lined, collapsed shaft along the Cuprite trend.

Cuprite mine development included a 291-m (954-ft) drift and a 20-m (65-ft) shaft sunk on the apex of the trend (Beeler, 1906; Currey, 1965). These workings encountered several small bodies of ore along the mineralized fault that reportedly consisted of native copper, cuprite, pyrite, chalcopyrite, and chalcocite with values in Au and Ag (Currey, 1965). Historic company reports showed 3–28 percent Cu, a trace to 2.56 fine ounces per ton Au, and a trace to 2 ounces per ton Ag (Currey, 1965). Three mineralized samples analyzed by McCallum and Houston (1985) showed values of 1–5 ppm Ag, 20–2,000 ppm As, 0.05–0.35 ppm Au, 70–700 ppm Co, and 0.02–0.12 percent Cu. However, little mineralization (≤ 0.08 ppm Au, 910 ppm Cr; WY-XRF ≤ 7 ppm Ag, ≤ 995 ppm Cr, ≤ 0.48 percent Cu, ≤ 137 ppm Ta, and ≤ 58 ppm Te) was found in samples of the Cuprite mine dump in 2017.

The Albany-Cuprite fault extends about 8 km (5 mi) southeast of the Cuprite mine, and sporadic mineralization occurs over nearly half of that distance (McCallum and Houston, 1985). The Bear mine, about 0.6 km (0.4 mi) southeast of the Cuprite mine in the E½ sec. 11, T. 14 N., R. 79 W., consists of a shaft sunk into a Cu-Au-bearing quartz vein in sheared and carbonated metagabbro. This part of the Albany-Cuprite trend cuts southeastward through the Horse Creek foliated granodiorite. No accounts of the Bear mining operation or production are known. However, assays on two chalcopyrite-malachite-rich samples with traces of native gold and molybdenite (Loucks, 1976) showed 0.04–1.5 ppm Au, 3.2–9.0 percent Cu, and 1–100 ppm Mo (McCallum and Houston, 1985).

Five 2017 samples (20170824NK-A through 20170824NK-E) from several prospect pits and one filled shaft (which may have been related to the Cuprite mine) between the Cuprite mine and the Bear mine showed WY-XRF ≤ 10 ppm Ag, ≤ 101 ppm As, ≤ 15 ppm Bi, ≤ 0.26 percent Cu, and ≤ 193 ppm Ta.

Prospects along the Albany-Cuprite fault approximately 2.4 km (1.5 mi) southeast of the Bear mine, in the SW¼ sec. 7, T. 14 N., R. 78 W., contain high values of Pt and Pd in addition to Au, Ag, and Cu (Loucks, 1976; McCallum and Houston, 1985; Hausel, 1989; 1997). These prospect pits expose thin quartz veins within a strongly sheared, lens-like portion of the fault zone that is about 30 m (100 ft) wide and extends approximately 0.5 km (0.3 mi). Some of the quartz veins are weakly mineralized with secondary Cu sulfides, malachite, limonite, and pyrite. Assays of two mineralized samples yielded 2.5–110 ppm Ag, 20–1,000 ppm As, 0.6–2.5 ppm Au, 0.1–15.6 percent Cu, 1.2–30 ppm Pd, and 5.5–40 ppm Pt (Loucks, 1976; McCallum and Houston, 1985; Hausel, 1989; 1997). Although these mineralized veins are hosted by sheared Horse Creek foliated granodiorite, McCallum and Houston (1985)

interpreted sheared mafic rocks along the fault zone to be the source for most of the precious and base metal values as suggested by the presence of Pd and Pt. A visit to these prospects in 2017 failed to indicate any mineralization.

A short prospect trench in the extreme northwestern corner of sec. 15, T. 14 N., R. 78 W., about 1.6 km (1 mi) west of the town of Albany, is another Pt-Pd occurrence investigated by McCallum and Houston (1985) that may (or may not) be related to the Albany-Cuprite trend. Magnetite-rich, spongy limonitic fault breccia in the older granite with xenoliths of the magnetite gabbro unit from the nearby Lake Owen complex apparently was worked for a short time, but no records of the operation are known. Limonitic concentrate from the trench averaged .058 ppm Pt, 1.2 ppm Pd, and as much as 500 ppm Mo, 700 ppm Pb and 1,000 ppm Zn (McCallum and Houston, 1985). McCallum and Orback (1968) interpret platinum enrichment of the breccia to result from leaching of these elements from sheared gabbro by hydrothermal fluids and redeposition with sulfides as breccia fragment matrix. This location was not visited in 2017.

A collapsed adit in the SE $\frac{1}{4}$ NW $\frac{1}{4}$ of the same section similarly was cut into an apparent mafic dike, or a large xenolith of the Lake Owen complex surrounded by the older granite. Heavy Fe-staining along with limonite, malachite, bornite, chalcopryrite, and chunks of pure magnetite are concentrated along fractures. Alteration slightly penetrates the surrounding granite. Analysis of sample 20170710NK-J showed 0.02 ppm Au, 28.2 ppm As, 0.28 ppm Pt, 0.306 ppm Pd, 1,300 ppm Cr, and 17.55 ppm U. WY-XRF further showed ≤ 13 ppm Ag, ≤ 141.6 ppm As, ≤ 4124 ppm Cr, ≤ 1876.3 ppm Cu, ≤ 636.8 ppm Pb, ≤ 1079 ppm Sc, and ≤ 162.9 ppm Te.

Mammoth trend

About 0.8 km (0.5 mi) north of and subparallel to the Florence trend is the Gold Crater mine and adjacent south-east-trending faults that comprise the Mammoth mineralized trend. The Mammoth trend cuts the Keystone Quartz Diorite and extends more than 8 km (0.5 mi) northwest into quartz-biotite gneiss (schist) and the Black Swan and Independence Cu-Au mines in the Keystone quadrangle. The trend also extends southeast for more than 1.8 km (1.1 mi) to the Mastodon mine. The Black Swan mine had reported values in Au, Ag, and Cu, with measurable Co, Pb, and Ni, along with traces of PGE (Loucks, 1976). The Independence mine hosted Au, Ag, Cu, and Bi, with traces of PGE (Beeler, 1906; Currey, 1965; Loucks, 1976). The Mastodon mine, which was not visited in 2017, is reported to be hosted by gabbro bodies within Keystone Quartz Diorite (Hausel, 1989), however, no information is available concerning mineralization at the mine.

The Gold Crater group (NE $\frac{1}{4}$ sec. 22, T. 14 N., R. 79 W.) consists of a series of shafts and interconnecting drifts along an east-trending andesite-dike-bearing fault. A shaft cutting a large quartz vein within the andesite dike initiated development of the Gold Crater mine. Later workings involved a mineralized lens-shaped quartz "seam" 13–46 cm (5–18 in) wide in a 350°-trending fault zone that reportedly carried Au ore averaging \$20 per ton (1890s prices) accompanied by very rich ore recovered locally from pyrite- and chalcopryrite-rich zones (Beeler, 1905). Samples from the Gold Crater workings showed enrichment in chalcopryrite, bornite, pyrite, hematite, and/or ankerite with variable amounts of galena and electrum (Loucks, 1976). Values obtained by McCallum and Houston (1985) from two samples showed 24–34 ppm Ag, 3.5–7.0 ppm Au, 0.5–6.6 percent Cu, and 150–500 ppm Pb. Last known activity in the Gold Crater mine was the driving of a 15-m (50-ft) drift in 1937 (Currey, 1965).

The Champion mine, immediately northeast of the Gold Crater, consists of a shaft and several prospect pits, and is part of the Gold Crater group of mines (Sutherland and Hausel, 1999). The mine was reported to carry values in both Au and Cu. Numerous other nearby prospects are scattered southeastward along faults, and up to 1.6 km (1 mi) eastward along the same andesite dike, which is found in the Gold Crater mine. Samples from the Gold Crater group and prospects along the fault (samples 20170810NK-A through ...D, and ...F through ...H) showed WY-XRF ≤ 10 ppm Ag, ≤ 446 ppm As, ≤ 1090 ppm Cu, ≤ 158 ppm Ta, ≤ 38 ppm Te, and ≤ 55 ppm Th.

Samples (20170809NK-C, ...D, and ...G; and 0170912NK-G, and ...H) collected from outcrops and prospects eastward along the andesite dike showed WY-XRF ≤ 9 ppm Ag, ≤ 434 ppm Ce, ≤ 1007 ppm Cr, ≤ 146 ppm Ta, and

≤9 ppm U. Chemical analysis of sample 20170809NK-B from the dike showed no significant concentrations of potentially economic metals.

Although most samples from historic developments along the Mammoth trend showed only minor mineralization, one prospect pit in altered Keystone Quartz Diorite, accompanied by epidote, quartz, and fault gouge (sample 20170810NK-E) showed 72.2 ppm Au (2.11 ounces per ton [opt]), 16.3 ppm Ag (0.48 opt), >250 ppm Bi, 7,720 ppm Cu, and 1.9 ppm Te. WY-XRF showed ≤5 ppm Ag, ≤498 ppm Bi, ≤3.33 percent Cu, ≤128 ppm Ta, and ≤19 ppm Te. The high Au values are probably due to the nugget effect within the sample, but suggest the potential for high-value mineralized pods along the trend.

Another southeast-trending fault, about 0.16 km (0.25 mi) north of the Gold Crater group, hosts the Endymion lode mine at the western edge of the quadrangle (Sutherland and Hausel, 1999) and a collection of collapsed adits, shafts, and prospects southeast of the Endymion. The Endymion shaft cuts fine-grained, epidotized, contorted mafic gneiss/schist, accompanied by slickensides, slightly vuggy and iron-stained massive quartz, and calcite. A composite sample of quartz and host rock (20170811NK-B) from the Endymion only showed WY-XRF ≤89 ppm Ta, but no other anomalous metals.



Figure 3. Collapsed adit southeast of the Endymion lode.

To the southeast of the Endymion, the shafts, adits (fig. 3), and prospects are cut into a mix of rock types, including contorted gneiss with iron-staining, quartz, epidote, cataclastically textured rock, and quartzite, accompanied by both mafic and felsic fine-grained debris. One shaft, collapsed at about 4.5 m (15 ft) below the surface, is cut by a vertical fracture zone trending due east. Composite sample 20170811NK-A from the shafts and adits showed 0.8 ppm Ag, 0.01 ppm Au, 234 ppm Pb, and 82 ppm W. WY-XRF showed ≤10 ppm (0.29 opt) Ag, ≤43 ppm (1.26 opt) Au, ≤2501 ppm Cu, ≤1247 ppm Pb, ≤144 ppm Ta, ≤26 ppm Te, and ≤2106 ppm W. The high metals values are probably due to the nugget effect within the sample, but again suggest the potential for high-value mineralized pods along the trend.

Vesuvius trend

Southeast-trending faults and shears north of the Mammoth trend and south of the Cuprite trend host several mines and prospects, including the Vesuvius lode (fig. 4). Quartz veins and epidote are common along the trend. The trend crosses the quartz-biotite gneiss and the contorted boundary gneiss, and extends into the Keystone Quartz Diorite.



Figure 4. Collapsed shaft and shaft house at the Vesuvius lode.

A composite sample from the Vesuvius lode (20170811NK-C) showed WY-XRF ≤10 ppm Ag, ≤1437 ppm Cr, ≤821 ppm Cs, ≤631 ppm Cu, ≤2531 ppm Sc, ≤165 ppm Te, and 1665 ppm V. Analysis of an epidote sample (20170811NK-E) containing sulfides from a

collapsed adit along the Vesuvius showed only traces of Au, Cu, and Pd. Part of the same sample showed WY-XRF ≤ 57 ppm As, ≤ 1013 ppm Cu, and ≤ 24 ppm Sn, but no other elevated metal concentrations.

Other prospects

Numerous other small mines and prospects are scattered within the Albany quadrangle, particularly in the western part. In general, these occur along a variety of dikes and veins, faults and shear zones, and within contact zones between differing rock types.

McCallum and Houston (1985) describe a small group of Cu-Au prospects in the SE $\frac{1}{4}$ sec. 13, T. 14 N., R. 79 W., and the SW $\frac{1}{4}$ sec. 18, T. 14 N., R. 78 W., in a wide, east- to southeast-trending shear zone that cuts Keystone Quartz Diorite. Small, mineralized quartz veins near the margins of the shear zone contain chalcopyrite, pyrite, and minor amounts of native Au. Assays of four samples yielded 1.0–28 ppm Ag, >2.5 –5.0 ppm Au, 0.01–16.5 percent Cu, 30–200 ppm Mo, and 200–500 ppm Zn. A 2017 sample (20170906NK-D) from a shaft near an obliterated adit in sec. 18 showed only WY-XRF ≤ 1005 ppm Cr.

Lake Creek district

In the southwestern corner of the Albany quadrangle, near Douglas and Muddy creeks, mineralization occurs in association with east-trending shearing in the Keystone Quartz Diorite. Seams of silicified mylonite in the wide sheared and altered zone exhibited Au-Cu mineralization, often accompanied by quartz veins (Currey, 1965; Hausel, 1989; 1997). Loucks (1976) also describe a sheared metapyroxenite dike within the shear zone.

Although the majority of development in the 1890s to early 1900s was just south of the Albany quadrangle, an obliterated shallow shaft adjacent to U.S. Forest Service Road 553, in SW $\frac{1}{4}$ NW $\frac{1}{4}$ sec. 2, T. 13 N., R. 79 W., is thought to have been referred to as Lake Creek mine 'C.' This was the northern-most, and one of the smaller, of several Au, Ag, Cu mines referred to as the Lake Creek mines (Sutherland and Hausel, 1999). When visited in 2017, a pit at the site showed pink to red iron-stained, northeast-trending shears in Keystone Quartz Diorite accompanied by slickensides and epidote with no quartz or apparent mineralization. Chemical analysis of a 2015 sample (20150818LC-12) from this site failed to show any anomalous metals content (Sutherland and Cola, 2016).

Lake Owen mafic complex

Investigations into the Lake Owen mafic complex as a potential source for PGE, Ni, and Cr began about 1976 (Loucks, 1976; Houston and Orback, 1976), with commercial interests noted in the 1980s and as late as 2007 (Rocky Mountain Resources Corp., 2007). Magnetite-rich layers, local pods, and lenses of magnetite as much as 15 cm (6 in) thick and several meters in length are abundant in the magnetite gabbro unit. An assay of magnetite from magnetite gabbro samples collected from exposures about 1.1 km (0.7 mi) west of the town of Albany showed greater than 1 percent Ti, 1,000 ppm Cr, 5,000 ppm V, 0.020 ppm Pt, and 0.035 ppm Pd (McCallum and Houston, 1985).

Anomalous amounts of PGE, Au, Ag, Ni, Cu, Cr, and V are reported from several units in the complex (Hausel, 2000). The highest Ni concentrations are in the olivine magnetite gabbro-norite unit, whereas maximum Pt values derived from samples in the layered unit (Loucks and Glasscock, 1989). Distribution of Cu within the complex appears to be random (McCallum and Houston, 1985).

Sulfides occur in some parts of the Lake Owen complex and are visible in layered unit sample 20170921NK-A. Chemical analysis of this sample showed no significant precious or base metals; WY-XRF ≤ 7 ppm Ag, ≤ 1234 ppm Cs, ≤ 362 ppm Cu, and ≤ 136 ppm Ta. Elemental analyses of four other Lake Owen samples (20170710NK-F, 20170711NK-B, 20170718NK-D, and 20170725NK-A) showed 0–1730 ppm Cr, 0–755 ppm Ni, 0–0.036 ppm Pd, and 0–0.04 ppm Te. WY-XRF of these and 14 other samples showed ≤ 7 ppm Ag, ≤ 34.3 ppm Au, ≤ 894 ppm Cr, ≤ 751.7 ppm Cu, ≤ 502 ppm Ni, and ≤ 129 ppm Ta.

Browns Park Formation

The Browns Park Formation hosts several prospect pits at scattered locations across the southwestern part of the quadrangle. Vine and Prichard (1959) describe Browns Park Formation uranium occurrences in the Miller Hill area of the southern Sierra Madre (about 80 km [50 mi] west-northwest of the Albany quadrangle) to be dominantly associated with silicified, brecciated limestones. Although no uranium mineralization was found in the Albany quadrangle prospects, all were dug into brecciated limestones and were interpreted to be uranium prospects. However, analyses of two of the limestone breccias (samples 20170720NK-C and 20170725NK-C) showed no U, 0.02 ppm Au, and 0.4–0.08 ppm Te. WY-XRF of these and three other samples showed ≤ 7 ppm Ag, ≤ 173 ppm La, and ≤ 205 ppm Ta.

REE

The Mesoproterozoic Sherman Granite near Albany was reported to contain elevated (greater than five times average crustal concentrations) concentrations of REE associated with disseminated allanite varying from 0.6 to 2.8 percent by volume (Dribus and Nanna, 1982; Mussard, 1982) with concentrations of La up to 198 ppm and Ce up to 328 ppm (King and Harris, 2002). Sutherland and Cola (2016) investigated these REE occurrences in 2015 and 2016, and of five samples collected in the area, only one hosted elevated REE. Sample 20150818LC-1, collected from altered Sherman Granite in a road cut within a northwest-trending shear zone exhibited 584 ppm Ce, 280 ppm La, 49.9 ppm Pr, and 164 ppm Nd. Another sample (20150818LC-12) collected from Lake Creek mine 'C' in an area also reported to host REE showed no elevated REE or other metals content (Sutherland and Cola, 2016).

The current study found elevated REE in Mesoproterozoic/Paleoproterozoic (?) pegmatite, sheared Paleoproterozoic older granite, felsic veins in a Paleoproterozoic andesite dike, the Paleoproterozoic Horse Creek foliated granodiorite, and in limestone breccia associated with the Miocene–Oligocene Browns Park Formation.

Analysis of a 2017 sample of pegmatite (20170719NK-C) showed 37.7 ppm Dy, 22.2 ppm Er, 24 ppm Gd, 7.75 ppm Ho, 3.86 ppm Lu, 5.2 ppm Tb, 3.66 ppm Tm, 268 ppm Y, and 25.8 ppm Yb. This sample also showed 5 ppm Ge, 18.4 ppm Hf, 110.5 ppm Nb, 16.9 ppm Ta, 28.8 ppm Th, and 0.02 ppm Te. WY-XRF of a separate piece of this sample indicated elevated Ce, La, and Y, along with elevated Nb, Ta, and ≤ 4 ppm Ag.

WY-XRF of sample 20170620WS-B from sheared older granite showed 1,577.5 ppm Ce and 533 ppm La, along with 124.7 ppm Nb, 80.9 ppm Ta, 183.4 ppm Th, and 20.3 ppm U. An unsheared sample of the older granite (20170710NK-K) showed WY-XRF values of ≤ 512.6 ppm Ce and ≤ 259.5 ppm La. WY-XRF of sample 20170824NK-O from mylonitic Horse Creek foliated granodiorite on Spruce Mountain showed ≤ 334 ppm Ce, and a composite sample (20170811NK-C) from a quartz vein cutting the Horse Creek at the Vesuvius lode showed ≤ 2531 ppm Sc. WY-XRF of dirty brecciated limestone/tufa (Sample 20170825NK-G) associated with the Browns Park Formation showed ≤ 173 ppm La along with ≤ 6 ppm Ag.

Critical and Strategic Elements

Elevated concentrations of individual CSEs are noted above in association with individual mines and mineralized trends. Both current and historic analyses suggest that should mining occur here in the future, associated recovery of minor amounts of CSEs might be possible.

DESCRIPTION OF MAP UNITS

Holocene alluvial deposits (Qal): These deposits include predominantly unconsolidated cobbles, gravel, sand, silt, and clay in channel deposits and in low-lying terrace deposits associated with active drainages. Alluvial deposits may include eluvial deposits, slope wash and some colluvial deposits, particularly in the northern part of the quadrangle.

Holocene colluvium (Qc): This unit consists of heterogeneous, angular to subangular colluvial debris that includes solifluction bodies, locally derived talus, and protalus ramparts in the canyon of the Middle Fork of the Little Laramie River in the northern part of the quadrangle.

Holocene landslide debris (Qls): This unit includes locally derived jumbled masses of angular debris accumulated by slump, creep, and rockfall on moderate to steep unstable slopes. It is topographically irregular to hummocky with small ponds common in depressions. Most landslides in the Albany quadrangle appear to involve Browns Park Formation that has moved in response to slip planes in clay layers of the underlying White River Formation.

Holocene–Pleistocene terrace/pediment deposits (Qtg): Boulders, cobbles, gravel, sand, and silt cover terraces and pediment-like surfaces along mountain flanks and drainages. These are defined after Blackstone (1970) and McCallum and Houston (1985). Quartzite with variable amounts of felsic gneiss, granite, and mafic rocks dominates the lithology in these deposits.

Holocene–Pleistocene upland gravels (Qg): Upland surfaces are veneered with 12–61 m (40–200 ft) of sub-rounded to well-rounded quartzite gravel, cobbles, and boulders up to 3 m (10 ft) in diameter in the northern part of the quadrangle (McCallum, 1964; McCallum and Orback, 1968; Coalson, 1971). The quartzites appear to be derived from the lower Proterozoic Libby Creek Group in the Snowy Range, approximately 20 km (12.4 mi) to the north (Houston and others, 1968). Although quartzites dominate, a wide variety of other lithologies are present in much smaller amounts. Extensive chatter marks on some boulders and cobbles suggest glacial derivation and therefore Pleistocene age.

Quaternary and/or Neogene–Paleogene deposits, undivided (QTu): Undivided Quaternary and/or Neogene–Paleogene deposits are primarily in areas of low relief covered with cobbles and gravel. Poor exposures provide insufficient information to determine the position of these deposits either within the White River Formation, Browns Park Formation, or within Quaternary upland gravels. This designation may also include other alluvial, colluvial, and terrace deposits.

Miocene–Oligocene Browns Park Formation (Tbp): McCallum and Houston (1985) refer to these rocks in the southeastern Medicine Bow Mountains as the North Park Formation. Re-evaluations by Snyder (1980) and Montagne (1991) indicate that these and equivalent rocks in the Saratoga Valley and the Sierra Madre are probably all Browns Park Formation. Love and others (1993) similarly eschew the name North Park Formation in Wyoming. Lilligraven (1993) did not identify the Browns Park Formation in the northeastern and southeastern Medicine Bow Mountains, but notes possible Oligocene strata, tentatively extending up into the Miocene. In the western Sierra Madre, he depicts the Browns Park Formation as Miocene, but extending down into the upper Oligocene.

The Browns Park Formation is variable in lithology and includes tan, gray, and olive drab calcareous to siliceous sandstone and siltstone, with some thin limestones and white pumicite beds (Luft, 1985; Montagne, 1991). A loosely consolidated, cross-bedded and sandy, ferruginous conglomerate containing Precambrian boulders up to 1 m (3 ft) in diameter is prominent near the base of the formation in the Saratoga Valley where the formation exceeds 732 m (2,400 ft) in thickness (Montagne, 1991). In the vicinity of the Albany quadrangle, the basal layer varies from an angular arkosic conglomerate to a silica-cemented breccia-like layer with large, up to 5 cm (2 in), angular pieces of Medicine Peak quartzite.

The Browns Park Formation includes apparently unconsolidated mafic-rock-rich gravels in the Cinnabar Park area in the northwestern part of quadrangle. In the southwestern part of the quadrangle, these overly scattered occurrences of arkosic limestone and/or white to gray, medium- to coarse-grained quartz sandstone, arkosic sandstone, and conglomeratic sandstone. Several outcrops of Browns Park Formation within the quadrangle include limestone layers up to several feet thick. The character of the limestone varies from massive to thin bedded and sandy to arkosic, brecciated, and in some places silicified.

In the Miller Hill area, west of the Sierra Madre and about 80 km (50 mi) west-northwest of the Albany quadrangle, the Browns Park Formation hosts uranium deposits, mostly associated with silicified limestone (locally brecciated and replaced by chalcedony; Vine and Prichard, 1959). Several prospect pits are found associated with the limestones within the Albany quadrangle, but no uranium mineralization was found in these.

Miocene–Oligocene limestone and tufa associated with the Browns Park Formation (Tbl): Limestones within the Browns Park Formation, mapped in 2017, are lime-cemented arkose and breccias, partially silicified limestone, cross-bedded sandy limestone, and tufa, interpreted to be related to hot springs activity (figs. 5 and 6). In some places, these appear to lay directly on top of Precambrian rocks. At other locations, stratigraphic positioning cannot be determined due to poor exposures.

In the Miller Hill area of the Sierra Madre, Love (1953) and Vine and Prichard (1959) reported opal, gray to brown chalcedony, calcite, and uranophane in travertine-like coatings on brecciated, silicified, and weathered limestone fragments, and as vug and joint fillings in the Miocene Browns Park Formation. These descriptions also indicate possible hydrothermal activity during or after deposition of the Browns Park Formation.

Currey (1965) notes shallow prospect pits in siliceous limestone (which he refers to as freshwater limestone) up to 3 m (10 ft) thick in the NW¼ of sec. 5, T.13 N., R. 78 W. Examination of this outcrop during the current project showed two prospects in limestone; one immediately south of a 137°-trending brittle shear zone in metavolcanic/metasedimentary gneiss and another about 67 m (220 ft) to the southwest. The limestone is light gray to white, massive (one layer up to 2 ft [0.6 m] thick) to thin bedded and sandy with possible cross-bedding in one area, and brecciated in places, erratically accompanied by felsic clasts up to 15 cm (6 in) across. Silicification of the limestone is variable and most obvious inside of broken pieces; neither chalcedony nor opal was found. This outcrop of about 0.4 ha (1 ac) hosts both massive limestone and breccia/tufa that appears characteristic of a hot spring deposit. WY-XRF of samples 20170725NK-B, ...C, and ...E showed about 1.6–19.6 percent Si, up to 55 ppm As, up to 5 ppm Ag, up to 205 ppm Ta, and up to 14 ppm Th; no U, such as described for the Miller Hill area, was detected.

A limestone outcrop in the SW¼ sec. 30, T. 14 N., R. 78 W., shows similar characteristics to that in sec. 5, T. 13 N., R. 78 W. McCallum and Houston (1985) note limestone in the Browns Park Formation in the SW ¼ sec. 26 and in sec. 35, T. 14 N., R. 79 W. (neither of these sites were visited in 2017). Scattered pieces of limestone from the Browns Park Formation were also noted in a series of shallow prospect pits along a southeast trend near a contact with the Keystone Quartz Diorite in the SW¼ sec. 23, T. 14 N., R. 79 W.

Oligocene–Eocene White River Formation (Twr): Lilligraven (1993) describes the White River Formation as upper Eocene in the northeastern and southeastern Medicine Bow Mountains, but as Eocene to lower Oligocene in some areas in Wyoming to the north and east. Love and others (1993) depict the White River as Oligocene only, while Love and Christiansen (1985) show a White River age of 31–35 Ma, extending from late Eocene into early Oligocene.



Figure 5. Limestone with felsic breccia in the Browns Park Formation.



Figure 6. Brecciated limestone tufa in the Browns Park Formation.

The White River Formation consists of white to buff and tan, poorly cemented, tuffaceous, fine-grained siltstone, clay, and shale with minor amounts of angular igneous and metamorphic rock fragments (Swetnam, 1961; Houston and others, 1968; Montagne, 1991). The scattered presence of small black to gray, tan, and white agates and opal within silicified ash or limestone (fig. 7) near the top of the formation helps distinguish White River Formation outcrops from the Browns Park Formation.

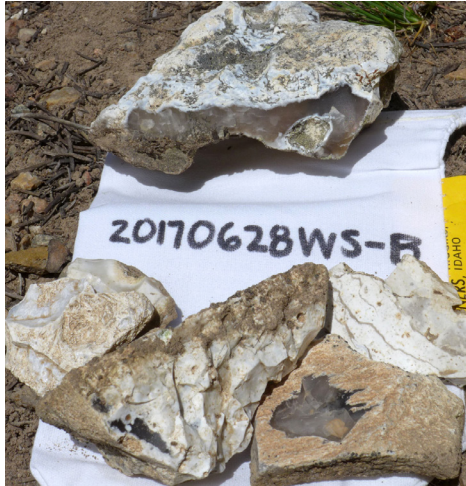


Figure 7. Agate and opal pieces characteristic of the White River Formation

Clay layers within the White River Formation are less permeable than the sand and conglomerate in the overlying Browns Park Formation, thereby producing springs at the contact, such as at the headwaters of Curitan Creek, just east of Cinnabar Park. These clay layers also appear to provide slip planes for landslides in the Albany quadrangle and adjacent areas. Although the White River Formation is poorly exposed, minor clay layers that crop out in scarps and drainages, along with pieces of characteristic silicified materials, support this conclusion.

The White River Formation is well exposed approximately 1.6 km (1 mi) east of Albany in the Lake Owen quadrangle in several locations, particularly along the right-of-way for Wyoming State Highway 11 (Houston and Orback, 1976). The best, although quite small, exposure of the White River Formation within the quadrangle is at the head of a landslide in sec. 25, T. 15 N., R. 79 W., in the northwestern corner of the quadrangle. Blocks and fragments of this unit also occur within landside debris in sec. 15 and 22, T. 14 N., R. 78 W.

Upper Cretaceous Steele Shale (Ks): The Steele Shale is predominantly dark-gray marine shale, interbedded in the upper part with thin beds of fine-grained, buff to orange-weathering, brown sandstone, and siltstone. The lower part of Steele Shale is exposed in the northeastern corner of the quadrangle. The thickness of the formation to the east in Centennial Valley has been estimated at 823 m (2,700 ft) by Houston and Orback (1976), where a persistent sandstone, 396 m (1300 ft) above the base is locally referred to as the Shannon Sandstone (Blackstone, 1970).

Upper Cretaceous Niobrara Formation (Kn): The Niobrara Formation is composed of an estimated 152 m (500 ft) of highly fossiliferous, predominantly gray, calcareous shale, interbedded with cream to yellow and orange-weathering silty limestone. Oyster shells (*Pseudoperma congesta*) almost entirely comprise some thin beds in the upper part of the formation (Houston and Orback, 1976). The thickness of the Niobrara Formation is estimated to be 85 m (280 ft) in the adjacent Lake Owen quadrangle (Houston and Orback, 1976) and 152 m (500 ft) in the Centennial Valley to the northeast (Blackstone, 1970).

Upper Cretaceous Frontier Formation, Upper Cretaceous Mowry Shale, and Lower Cretaceous Thermopolis Shale undivided (Kft): The estimated maximum thickness of these combined units is 210–279 m (690–915 ft).

The Frontier Formation is dominated by about 140–183 m (460–600 ft) of gray to black shale with interbedded bentonite beds and siderite septarian concretions that are most abundant near the base. The Wall Creek Sandstone, near the top of the Frontier Formation, includes as many as three thin discontinuous sandstone layers with a cumulative thickness of about 3 m (10 ft); these contain black chert pebbles and common shark and ray teeth (Houston and Orback, 1976).

The Mowry Shale consists of about 37–50 m (120–165 ft) of dark-gray to black, siliceous, silver-gray-weathering shale with common fish scales and little vegetative cover. The Mowry Shale hosts numerous thin bentonite beds, particularly near the top of the formation (Blackstone, 1970; Houston and Orback, 1976).

The Thermopolis Shale is about 34–46 m (110–150 ft) of black to dark-brown marine shale with brown to olive-green, fine-grained sandstone layers that host bedding planes covered with tubular structures interpreted as worm burrows (Blackstone, 1970; Houston and Orback, 1976). The Muddy Sandstone Member, at the top of the formation, consists of about 6 m (20 ft; Blackstone, 1970) of clean, gray to brown, medium-grained sandstone containing abundant black chert grains mixed with white quartz and chert. The Muddy Sandstone Member also hosts fragments of charcoal in both the sandstone and adjacent shale (Houston and Orback, 1976).

Lower Cretaceous Cloverly Formation (Kcv): With an overall thickness of about 52 m (170 ft), the Cloverly Formation consists of an upper reddish-brown to yellow, iron-stained, thin-bedded sandstone, a middle pink shale and gray to pink siltstone, and a basal, locally conglomeratic, cross-bedded, white sandstone. Some of the sandstones are silica cemented to form orthoquartzites, and the basal conglomerate locally hosts pebble-sized clasts of quartz and chert (Blackstone, 1970; Houston and Orback, 1976;). The Cloverly Formation unconformably overlies the Morrison Formation.

Upper Jurassic Morrison and Sundance Formations undivided (Jms): The Morrison Formation comprises white sandstone beds near the top underlain by bluish-gray, purple, deep red, and gray shale that contains lenticular beds of white, cross-bedded, fine-grained sandstone and gray nodular limestone. The formation totals about 91 m (300 ft) in thickness, hosts common fragments of green, red, gray, and purple chert, especially near the base, and locally contains calcareous nodules, bone fragments, and partial skeletons of reptiles (Blackstone, 1970; Houston and Orback, 1976).

The Sundance Formation is about 15 m (50 ft) thick and consists of white to pale yellow, crossbedded and ripple-marked, calcareous, glauconitic sandstone, and siltstone, with gray and green shale in the lower part. Abundant fossil *Pachyteuthis densus* (thick-walled belemnite rostrum) are found in the upper part. The lower contact is an unconformity (Blackstone, 1970; Houston and Orback, 1976).

Upper Triassic Jelm Formation and Triassic–Permian Chugwater Formation undivided (Tꞑꞑc): The Jelm Formation is 40–76 m (130– to 250 ft) of orange and red siltstone and sandstone overlying a distinctive clay-pebble conglomerate, which may include fragments of vertebrate bones and crocodile teeth (Houston and others, 1968; Love and others, 1993).

The Chugwater Formation consists of about 168–228 m (550–750 ft) of thinly bedded calcareous red shales, siltstones, and local thin sandstones with some thin beds of limestone and gypsum (anhydrite). The upper part of the Chugwater is referred to as the Red Peak Member of the Chugwater Formation (Blackstone, 1970; Houston and others, 1968; Houston and Orback, 1976; Love and others, 1993). The lower part of the Chugwater Formation is Permian and contains thin beds of gray to white limestone and gypsum (Ver Ploeg and others, 2016).

Permian Forelle Limestone, Satanka Shale, and Permian-Pennsylvanian Casper Formation undivided (PIPꝼc): The Forelle Limestone, at the top of the Satanka Shale, is a distinct and resistant 3–6 m (10–20 ft) thick, lavender to gray and white, crenulated limestone that often contains thin red to gray shale or siltstone in the middle (Houston and others, 1968; Blackstone, 1970; Houston and Orback, 1976). The Satanka Shale comprises 37–67 m (120–220 ft) of orange to red siltstones and shales that contain thin lenticular beds of gypsum, limestone, and ferruginous sandstone (Houston and others, 1968; Blackstone, 1970; Houston and Orback, 1976).

The approximately 63-m-thick (207 ft) Casper Formation consists of an upper yellowish to pink, buff, and white, fine- to medium-grained, calcareous, cross-bedded sandstone with well-developed festoon crossbedding and abundant orange chert grains. The middle of the formation is red and gray, hard siltstone and shale with some thin gray limestone beds. The lower part of the Casper Formation is white and red, cross-bedded sandstone that is conglomeratic at the base (Houston and others, 1968; Blackstone, 1970; Houston and Orback, 1976).

Pennsylvanian Fountain Formation (Pf): The Fountain Formation varies from about 122 m (400 ft) to more than 152 m (500 ft) of predominantly pink to maroon, calcareous, arkosic sandstone with lesser beds of light-purple arkose, gray sandstone, red siltstone, red shale, and white limestone, with a few interbedded conglomerates. Beds within the formation are discontinuous and variable in thickness, channels filled with cross-bedded sandstone and/or conglomerate are common, and the lower contact marks a major unconformity (Houston and others, 1968; Blackstone, 1970; Houston and Orback, 1976).

Mesoproterozoic

Proterozoic dikes (Yd): McCallum and Houston (1985) describe these dikes as magnetite-rich, porphyritic quartz latite (or microgranite). Their color varies from pink to pink-orange to warm-toned gray. The Proterozoic dikes are very quartz rich, with most quartz undeformed and un-metamorphosed. These dikes also host small amounts of plagioclase, sphene, epidote, and biotite. The dikes are characteristically fine grained, but vary to medium grained, and although not dated, may be related to the Sherman Granite. No fabric was observed in any of the outcrops. They are predominantly found in the Lake Owen area and include some dikes described by Houston and others (1968) as granitic dikes that may be of more than one age and dikes of white to pink fine-grained rhyolite.

Sherman Granite (Ys): The Sherman Granite is a pink, medium- to coarse-grained, faintly foliated granite dated at $1,433 \pm 1.5$ Ma by Frost and others (1999). The Sherman is typically equigranular with medium-grained characteristics more abundant near contacts, but a younger coarse-grained porphyritic phase is also present (McCallum and Houston, 1985).

Contacts are typically sharp where older rocks are locally cut by sills and dikes of the Sherman Granite. Plagioclase, microcline, and quartz tend to be equicrystalline, but biotite is highly variable in size. Based on crystal form, some biotite appears to replace hornblende or tourmaline. Local hybridization of both granite (more abundant potassium feldspar) and country rock (more abundant amphibole and biotite) occurs where the granite is in contact with mafic hosts. Stretched and flattened xenoliths of earlier rock types are common but nowhere abundant. Where sheared and brecciated, the Sherman Granite is locally enriched in epidote and quartz and is a very deep red, which could be confused with the older granite.

Mesoproterozoic/Paleoproterozoic (?)

pegmatite (YXp): Pegmatite is found throughout the quadrangle, but most veins and dikes are too small to map. The larger dikes crop out in the south central part of the quadrangle, cutting, or cropping out in the vicinity of, the Lake Owen layered mafic complex. The pegmatites are generally conformable to the foliation of the rocks into which they intrude (McCallum and Houston, 1985) and may be of more than one age (Houston and others, 1968).

These pegmatites are pink to white and consist primarily of quartz, microcline, and muscovite, locally accompanied by abundant small garnets. Crystal sizes range from 0.2–30 cm (0.08–12 in). Sharp chilled margins and alternating layers of fine and coarse crystals on the outer edges of the pegmatites are notable (fig. 8).



Figure 8. Pegmatite with chilled margins and alternating layers of fine and coarse crystals.

Chemical analysis of pegmatite sample 20170719NK-C showed elevated concentrations of REE, including Dy, Er, Gd, Ho, Lu, Tb, Tm, Y, and Yb. In addition, this pegmatite contained 5 ppm Ge, 18.4 ppm Hf, 110.5 ppm Nb, 16.9 ppm Ta, 28.8 ppm Th, and 0.02 ppm Te.

Houston and others (1989) report Rb-Sr isochrons for pegmatites in other parts of the Medicine Bow Mountains of $1,510 \pm 40$ Ma, $1,565 \pm 40$ Ma, and $1,620 \pm 40$ Ma, after Hills and others (1968). Immediately southeast of the Albany quadrangle, in the Woods Landing quadrangle, Campbell and Shelton (in press) provide a recent date on a pegmatite dike of $1,514 \pm 36$ Ma.

Paleoproterozoic

andesite dikes (Xsan): Although small dikes of this type occur, only one large east-trending dike has been depicted in the western and central part of the Albany quadrangle. It is a fine-grained, biotite-rich, pigeonite andesite that grades into hornblende-rich varieties, where some amphibole may be secondary. The dominant minerals are quartz, biotite, epidote, and plagioclase; quartz is red-brown in color, which deceptively gives the rock a strong mafic appearance. The major dike and similar smaller dikes intruded along fault zones, and are locally sheared and chloritized (McCallum and Houston, 1985). Shearing produced an obvious fabric comprising fracture planes and foliations.

Numerous prospect pits are found along this dike and are associated with similar dikes. Chemical analysis of 20170809NK-B showed traces of Au and Te, but no other anomalous elemental occurrences. WY-XRF of samples from the main andesite dike (20170809NK-C, ...D, and ...G; and 0170912NK-G, and ...H) showed elevated measurements of Ag, Ce, Cr, Ta, and U. Chemical analysis of 20170912NK-H showed no significant precious or base metals, but elevated Ba of 1,800 ppm. Several radiometric dating attempts were made on the large andesite dike. However, all zircons recovered from the samples were too metamict to give any meaningful results.

mafic intrusive rocks (XS): Mafic dikes and small irregular intrusions within the Albany quadrangle are most abundant cutting the eastern portions of the Keystone Quartz Diorite, just west of the edge of the Lake Owen layered mafic complex. The mafic dikes and small intrusions are variably metamorphosed, generally exhibit little or no fabric, are typically dark gray-green to black, less than 5 m (16 ft) thick (although much larger bodies occur), and fine to medium grained, but grade into coarse-grained phases. Some are fine grained and basaltic throughout, a few are gabbro and metagabbro, while others are diabasic with chilled margins. Alteration of the dikes is moderate to extensive, and locally, bodies are completely amphibolitized (McCallum and Houston, 1985).

The mafic dikes exhibit a broad range in mineral composition, from being very amphibole rich to very biotite rich, with varying amounts of plagioclase, quartz, and opaque minerals. McCallum and Houston (1985) found these dikes to contain 25–60 percent plagioclase (An 35–70) and 40–70 percent hornblende, which is locally actinolitic and commonly chloritized, accompanied by variable amounts of accessory biotite, magnetite, ilmenite, and epidote. Relict grains of clinopyroxene were recognized in some samples.

The mafic dikes are similar to diabase dikes that cut the Sherman Granite several kilometers to the south and southeast of the quadrangle that have been dated at 1,420 Ma by Ferris and Kreuger (1964); however, none are known to cut the Sherman Granite within the Albany quadrangle.

small felsic intrusives (Xgf): Small felsic intrusives are most abundant in the southern and eastern parts of the quadrangle. They appear somewhat consistently between differing rock types within the Lake Owen layered mafic complex and immediately west of the western edge the complex. Thin to irregular sills are especially abundant within the Keystone Quartz Diorite and in shear zones. Most sills are moderately uniform in thickness from 3–15 m (10–50 ft), are often continuous for hundreds of meters to more than 1 km (0.6 mi), and typically accentuate structural trends of their hosts. However, these rocks exhibit both concordant and discordant contact relationships and are interpreted as both syn- to post-shear intrusions (McCallum and Orback, 1968; Ramirez, 1971).

Mineralogically, the small felsic intrusives contain quartz, microcline, albite, and biotite, with occasional hornblende and magnetite/hematite. No fabric was observed in any of these intrusives, and crystal sizes generally range 1–5 mm (0.04–0.2 in), with minor coarse-grain occurrences.

older granite (Xg): This is a distinct red to orange, coarse-grained, foliated granite that crops out northwest of the Lake Owen layered mafic complex in the central part of the quadrangle. Houston and others (2003) equate it with quartz monzonite and similar rocks in other parts of the Medicine Bow Mountains. The granite is composed of about 60 percent plagioclase and potassium feldspar, with quartz, biotite, and magnetite (biotite and magnetite typically make up 10 to 15 percent). The granite hosts some xenoliths of the Lake Owen layered mafic complex. WY-XRF of the older granite (sample 20170710NK-K) showed slightly elevated concentrations of As, Ce, and La.

luxullianite (Xgl): The luxullianite is thought to be a late phase of the Rambler granite (McCallum and Orback, 1968; Coalson, 1971). It consists of generally concordant, locally zoned, medium-grained, pink to pinkish-white, tourmaline-rich (up to 30 percent), lenticular to pod- and dike-like bodies intruded into mylonite gneiss and amphibolitized metaigneous rocks near the Rambler Splay of the Mullen Creek-Nash Fork Shear Zone (Houston and McCallum, 1961; McCallum, 1964) in the northwestern part of the Albany quadrangle. The mineralogy, in order of relative abundance, includes plagioclase (albite), quartz, microcline, tourmaline, muscovite, sericite, and garnet. Black tourmaline (schorl) varies from microscopic needles in quartz to euhedral crystals several millimeters long (fig. 9) in aphanitic rocks, to crystals several inches long in pegmatitic phases (McCallum and Orback, 1968). Hills and Houston (1979) report a Rb-Sr whole rock isochron of $1,699 \pm 40$ Ma for the luxullianite, which could be revised using more precise modern techniques.



Figure 9. Luxullianite with black schorl crystals.

Rambler granite (Xgr): McCallum (1964) and Houston and others (1968) describe the Rambler Granite from granitic rocks recovered in underground workings at exposures in the vicinity of the New Rambler mine approximately 2.5 km (1.5 mi) west of the Albany quadrangle. It is exposed only in the northwestern corner of the quadrangle where it

is a medium- to coarse-grained, pink to red, microcline-rich granite that is cataclastically foliated with abundant epidote along shear planes. It consists of quartz, potash feldspar, sodic plagioclase, biotite, and chlorite with minor amounts of epidote, hornblende, muscovite, magnetite, and allanite (McCallum and Orback, 1968; Coalson, 1971). The Rambler granite exhibits both conformable and crosscutting relationships with surrounding rocks. Hills and Houston (1979) date this granite for a Rb-Sr whole rock isochron of $1,730 \pm 15$ Ma. Premo and Loucks (2000) more recently reported a date of $1,770.8 \pm 3.4$ Ma for the Rambler granite.

cataclastic textured rocks (Xmc): These rocks are observed in the west-central and northwestern parts of the quadrangle, and generally include fine-grained rocks within shear zones where original rock type and character could not be determined. These cataclastic rocks exhibit variable weathering textures ranging in appearance from almost sandy or shaly to phyllite and mylonite. Silicification and jasperization are common.

mixed units within the Rambler Splay of the Mullen Creek-Nash Fork Shear Zone (Xmx): Various rock type slivers, and sheared to mylonitic rocks crop out within the Rambler Splay of the Mullen Creek-Nash Fork Shear Zone. These include rocks described by McCallum and Houston (1985) as calc-silicate gneiss, marble, amphibole gneiss, quartzofeldspathic gneiss, mylonitic gneiss, and others. Outcrops of these various rocks are combined due to small outcrop sizes coupled with poor exposures.

mylonitic gneiss (Xmy): The mylonitic gneiss occurs in the northwestern part of the quadrangle immediately southeast of the Rambler splay of the Mullen Creek Nash Fork Shear Zone (Houston and others, 1968). It is a distinct, generally pink to buff or gray, locally black, very fine- to medium-grained gneiss with moderately to well-developed

cataclastic to mylonitic fabric and pronounced flow structure (fig. 10). Very fine-grained rocks exhibit the strongest mylonitic fabric. The gneiss is predominantly felsic in nature but includes lenses, stringers, and layers of mafic rock, particularly in the western part of the Albany quadrangle. Porphyroclasts of quartz and potassium feldspar (microcline) are common as are augen and lenses of polygonised quartz (McCallum and Houston, 1985).

The mylonitic gneiss is highly variable mineralogically, but generally is quartz rich with approximately equal amounts of potassium feldspar and plagioclase (commonly oligoclase to sodic andesine), accompanied by significant biotite, which is locally chloritized. Accessory minerals include magnetite-ilmenite, epidote, titanite-sphene, and muscovite (McCallum and Houston, 1985).



Figure 10. Typical broken surface of mylonitic gneiss.

Lake Owen layered mafic complex: The Lake Owen layered mafic complex is a large, roughly circular, intermittently layered mafic intrusion of approximately 54 km² (21 mi²) consisting of gabbro, olivine gabbro, norite, olivine norite and troctolite, all locally gradational with one another. The complex is a relatively unaltered and undeformed concave, semicircular structure that dips steeply to the east and northeast. It cuts adjacent gneiss units and the Keystone Quartz Diorite on its western flank, and is cut by the Sherman Granite to the north. Rocks within this complex are the least altered of any mafic rocks in the Medicine Bow Mountains, although some units along the southern border of the complex are partially amphibolitized. A date from pegmatitic gabbro-norite pods (sample 20170921NK-A) within the layered unit yielded a U-Pb zircon age of 1775.1± 3.0 Ma.

Loucks and Glasscock (1989) note 18 cyclic units within the Lake Owen layered mafic complex that were defined by large-scale repetitions of two or more lithologic units and by compositional variations in the rock mineralogy. Of these, at least 12 stratigraphic horizons in the complex exhibit cumulus sulfide mineralization. Shearing and brecciation between some layers in the Lake Owen complex, plus the injection of felsic dikes parallel to some layers suggest a complicated origin for the layered mafic complex.

Subunits and layering within the Lake Owen layered mafic complex have been variably defined (Houston and Orback, 1976; Houston and others, 1968; McCallum and Houston, 1985; Patchen, 1987; Houston and others, 2003), but differences are generally subtle and rock types within each layer may be highly variable. Several of these subunits occur repetitively within the complex, whereas a few occur only once. The following subunit descriptions are based on McCallum and Houston (1985) and Houston and others (2003) in combination with field observations in 2017.

- **olivine magnetite gabbro-norite (Xlu):** Olivine magnetite gabbro-norite is dark-gray to black with highly variable magnetite content ranging from 3–28 percent, but averaging about eight percent (Houston and others, 2003).
- **magnetite gabbro-norite (Xlr):** The magnetite gabbro-norite is dark gray to purple, with a higher proportion of mafic minerals than gabbro-norite, and includes 7–15 percent cumulate magnetite (Houston and others, 2003). Magnetite gabbro-norite within this unit is dominant but is interlayered with gabbro-norite.
- **norite (Xln):** The norite is dominantly gray, varying to orange, medium to coarse-grained, and varies from unlayered to subtly layered. Layering, where present, results from alterations of plagioclase- and pyroxene-rich layers, and preferred orientations of plagioclase. Orange weathering is attributed to hematite plates in the pla-

gioclase (Houston and others, 2003). Pyroxenes in the norite tend to be characteristically green throughout the rock, and are dominantly lengthened along the c-axis, an attribute only observed in the norite and gabbro-norite.

- **gabbro (Xlg):** The gabbro is dark gray to greenish-black, to orange-weathering, and medium to coarse grained. In general, plagioclase laths are preferentially oriented, and the rock typically hosts a lower magnetite content than other units within the complex (McCallum and Houston, 1985).
- **troctolite (Xlt):** This light-gray to gray unit is dominated by troctolite and exhibits well-developed preferred orientation of plagioclase laths. Oxidation of large olivine crystals results in localized brownish-red spotted textures. Interlayers of anorthosite and leuconorite are common within the troctolite (McCallum and Houston, 1985).
- **olivine gabbro (Xlo):** Olivine gabbro is dark gray to reddish-brown, and fine grained. It forms relatively resistant ridges within the Lake Owen layered mafic complex. The olivine is not always obvious in hand sample where it has not been oxidized. Grain size becomes coarse near the top of the unit (Houston and others, 2003). Plagioclase laths have a strong preferred orientation. Olivine in weathered samples typically alters to dark brown and locally leaves voids where the mineral is partially to completely destroyed (McCallum and Houston, 1985).

- **layered unit (Xll):** The layered units consist of alternating light and dark layers of olivine gabbro-norite, troctolite, and norite, varying in thicknesses from a few centimeters to a few meters (about 1 in to 10 ft). These units include some cyclical layers of olivine gabbro-norite alternating with layers of norite. Magnetite is common within the layered units. The layered units are generally continuous along strike and hypothesized to result from slow, steady convective overturn (McCallum and Houston, 1985) in contrast to cyclical layers that are thought to result from rapid convective overturn (Wagner, 1968). Cyclical layers and lenses, which are part of the layered unit, exhibit gradational changes in crystal size from fine to pegmatitic (<1 mm to 4 cm; <0.04 in to 1.6 in) over short distances (fig. 11) and locally are accompanied by sulfides. A sample (20170921NK-A) of the pegmatitic phase was collected for radiometric dating, with results given above.



Figure 11. Sample 20170921NK-A, gabbro-norite within the Lake Owen layered unit showing changes in crystal sizes.

- **gabbro-norite (Xlgn):** The gabbro-norite hosts dark-brown, dark-gray, and common black mineral-graded layers with dark pyroxene bottoms overlain by light plagioclase-rich tops. These layers are separated by thicker gabbro-norite with preferred mineral orientations, but no distinct layering. Magnetite gabbro layers are also present, particularly near the top (Houston and others, 2003). Plagioclase color varies from a smoky purple to a deep, dark gray. The gabbro-norite hosts both ortho- and clinopyroxene in variable ratios, accompanied by hornblende and sphene.
- **magnetite gabbro (Xlm):** The magnetite gabbro is dark brown to purplish-gray and black, and magnetite-rich, generally containing more than 10 percent magnetite. This unit is consistently equicrystalline with blocky, stubby crystals of about 1–3 mm (0.04–0.1 in). Disseminated magnetite within the layer is dominant, but distinct layers and lenses of massive magnetite up to 30 cm (12 in) or more thick also occur. Although much of the

magnetite appears to be a cumulate mineral phase, it also occurs interstitially, in microveinlets, and/or replacing silicate minerals where it comprises greater than 15 percent of the rock (McCallum and Houston, 1985).

- **border phase (Xlb):** The border phase consists of dark-gray to black and porphyritic basalt, which is locally brecciated and filled with gabbro, and exhibits the effects of contact metamorphism (Houston and others, 2003) and mixing with adjacent rock types at the base (particularly the Keystone Quartz Diorite). Its overall appearance varies from that of a breccia, a gneiss, or a solid unit of basalt. It is epidote rich and often has felsic veining. The gneissic appearance in the border phase is shown in fig. 12.



Figure 12. Lake Owen border phase gneiss with xenoliths.

Horse Creek foliated granodiorite (Xgh):

The Horse Creek foliated granodiorite crops out in the northwestern part of the Albany quadrangle and is widespread within the Keystone quadrangle immediately to the west. It occurs as a sill-like body, but interfingers along foliation planes of older gneiss units as well as in rocks of the Mullen Creek layered mafic complex (Sutherland and Hausel, 2005b). Extreme variations within parts of this unit probably resulted from gradational interactions with surrounding units and cataclasis; these variations also contributed to a diversity of names applied to the unit.

The granodiorite is generally pink to buff, or light gray in color, taking on a greenish cast where epidote is abundant. It is dominated by plagioclase (andesine to calcic oligoclase), along with quartz, potassium feldspar (mostly perthitic), and biotite. McCallum and Orback (1968) observed a general trend in the unit from microcline-rich in the east to microcline-poor in its western outcrops. Accessories include muscovite, epidote, and minor hornblende, magnetite, ilmenite, titanite-sphene, and allanite (McCallum and Orback 1968). The Horse Creek foliated granodiorite is predominately fine- to medium-grained, with lesser coarse-grained phases (fig. 13). This unit varies from unfoliated to conspicuously foliated (fig. 14), with zones of moderate to severe cataclasis (McCallum and Orback 1968). Foliation primarily results from alignment of biotite, and/or muscovite locally, and secondarily from cataclasis proximal to the Rambler Splay of the Mullen Creek-Nash Fork Shear Zone.



Figure 13. Medium- to coarse-grained Horse Creek foliated granodiorite with mafic xenolith at top.



Figure 14. Typical foliation within the Horse Creek foliated granodiorite.

The Horse Creek foliated granodiorite includes parts of Houston and others' (1968) older granite and quartzo-feldspathic gneiss, Currey's (1965) quartz-feldspar gneiss, and McCallum and Houston's (1985) biotite-plagioclase gneiss, with which the contact may in part be gradational. This unit has also been referred to by Houston and others (1989) as the Horse Creek granite, which Premo and Van Schmus (1989) report as having a U-Pb zircon age of $1,777 \pm 4$ Ma. Additional information on this unit can be found in Sutherland and Hausel (2005a, b).

Mullen Creek layered mafic complex (Xc): The Mullen Creek layered mafic complex is a large, irregularly shaped body of fine- to coarse-grained mafic igneous and metaigneous, locally layered rocks south of the Cheyenne belt, most of which occurs to the west of the Albany quadrangle. It is tilted on edge, and has more than 21 cyclic units based on petrographic analyses, which resembles the stratigraphy of the Lake Owen layered mafic complex (Loucks and Glasscock, 1989), but is much more metamorphosed and deformed. Primary rock types within the complex include gabbro, olivine gabbro, norite, leucogabbro, anorthosite, diorite, basalt/diabase, and pyroxenite, along with completely amphibolitized products. Loucks and others (1988) calculated a U-Pb zircon age of $1,777.6 \pm 2.1$ Ma from a diorite within the complex. Further information on the Mullen Creek layered mafic complex can be found in Sutherland and Hausel (2003).

The Mullen Creek layered mafic complex is cut by the Horse Creek foliated granodiorite along part of its eastern margin, but appears conformable with quartz-biotite gneiss and possibly other rock units. Contact relationships are commonly obscured by emplacement of lenticular masses of granitic material and by poor exposures. The northeastern edge of the complex is truncated by the Rambler Splay of the Mullen Creek-Nash Fork Shear Zone, with which small elongated slices of it are associated in the northwestern part of the Albany quadrangle (Houston and others, 1968; McCallum and Houston, 1985; Houston and others, 1989).

Within the Albany quadrangle, the rocks of the Mullen Creek layered mafic complex are commonly sheared, partially to completely amphibolitized, and mineralogically dominated by hornblende, actinolite, talc, and plagioclase. Principal accessories are chlorite, magnetite, ilmenite, epidote and/or clinozoisite, sphene (titanite), and allanite (McCallum and Houston, 1985).

metavolcanic and metasedimentary gneiss and schist (Xv): This highly variable unit is found only near the south-central edge of the quadrangle. It is described as a quartz-andesine gneiss by Currey (1965), and as interlayered amphibolite-grade metavolcanic and metasedimentary gneiss and schist by Houston and others (2003). It consists of fine-grained, highly foliated, light- to dark-gray to deep orange-pink and light-pink gneiss composed principally of potassium feldspar, quartz, plagioclase, hornblende, biotite, and accessory epidote, with hornblende in greater abundance than the biotite. Banding within the unit is pronounced where composition cycles between mafic and felsic. Lateral variations between dominating mafic and felsic components are also common, but irregular in extent. Foliation varies from slightly noticeable to strong, with cataclastic textures found throughout the unit. Shearing, both brittle and ductile, is most significant in and adjacent to a major east-trending shear zone near the southern edge of the quadrangle. Rhyolite from this unit, in the adjacent Foxpark quadrangle to the south, is dated at $1,778.4 \pm 1.7$ Ma (Carnes and others, in press).

Keystone Quartz Diorite (Xk): The Keystone Quartz Diorite (fig. 15) is a medium- to light-gray, whitish-gray to pink, medium- to coarse-grained quartz diorite found east, south, and west of the Lake Owen layered mafic complex (Currey, 1965; Houston and others,



Figure 15. Typical freshly exposed Keystone Quartz Diorite.

1968). The rock is locally porphyritic, weakly to strongly foliated (both primary and secondary), and crops out as prominent massive, rounded to spheroidal blocks bounded by widely spaced joints. Composition is dominated by plagioclase (~50–70 percent) with roughly equivalent amounts of quartz and up to 30 percent hornblende. Accessory biotite, epidote, chlorite, microcline, and titanite-sphene occur in variable amounts up to 10 percent. The composition tends to be more felsic to the west and southwest where microcline is more abundant and plagioclase tends to be more sodic (Houston and others, 1968).

Contacts between the quartz diorite and adjacent pre-existing metamorphic rocks are often gradational. Houston and others (1978) report that the quartz diorite is younger than adjacent quartz-biotite gneiss and amphibole gneiss. Houston and others (2003) describe interlayering with felsic gneiss in the Lake Owen area. Campbell and Shelton (in press) provide a U-Pb zircon age for the Keystone Quartz Diorite of $1,784.7 \pm 1.9$ Ma from the Woods Landing quadrangle, immediately southeast of the Albany quadrangle.

Keystone Quartz Diorite transition zone (Xki): Contacts between the Keystone Quartz Diorite and adjacent pre-existing rocks are often gradational through a transition zone that varies from a few cm to greater than 183 m (600 ft) wide (Currey, 1965; Sutherland and Hausel, 2005b; Houston and others, 2003). Grain size within the quartz diorite decreases and foliation becomes stronger when nearing the contact; schlieren of host hornblende- and/or biotite-rich gneisses and schists are common. The quartz diorite partially replaces, incorporates breccia, or is injected into the folia of older rocks within the transitional contact (fig. 16). Numerous inclusions of the older rocks in the quartz diorite suggested to Currey (1965) that a stopping process contributed to emplacement of the quartz diorite. Xenoliths, sills, and lenticular bodies exhibit varying degrees of hybridization and locally comprise more than 30 percent of exposures (McCallum and Houston, 1985).



Figure 16. One of many variabilities within the Keystone Quartz Diorite transition zone.

contorted boundary gneiss (Xcbg): The contorted boundary gneiss is a distinct transition unit between the Keystone Quartz Diorite and the quartz-biotite gneiss extending eastward across the center of the quadrangle. This gneiss has very-fine crystals and foliations of about 1–2 mm (0.04–0.08 in), which may exhibit dramatic small-scale folds and crenulations. Coarser-grained felsic injections within the gneiss are common (fig. 17).

quartzofeldspathic gneiss (Xvf): This gneiss is variable in its composition and description, is locally sheared, and crops out in the southwestern part of the quadrangle. In general, the gneiss weathers to a very dark pink, but is light pink on fresh surfaces. It is mineralogically dominated by plagioclase, quartz, biotite, and epidote, accompanied by a trace of hematite/magnetite. The mafic content varies between 10 and 15 percent. The gneissic fabric tends to be weak, but obvious with underdeveloped foliations.

quartz-biotite gneiss (Xqb): Currey (1965) and Sutherland and Hausel (2005b) mapped this unit as quartz-biotite schist in the Keystone quadrangle to the west, where it is 732 m (2400 ft) thick. The schist is gray to black to pinkish-gray and brown where weathered. It is dense, laminated, and generally very fine-grained with variable schistosity.

Within the Albany quadrangle, this unit is more gneissic than schistose, and is dominated by biotite and quartz with variable amounts of plagioclase (oligoclase-andesine) and potassium feldspar, opaque minerals, epidote,

muscovite, chlorite (after biotite), amphibole, and titanite-sphene (McCallum and Houston, 1985). Potassium feldspar and muscovite tend to be more abundant in easterly exposures.

The gneiss is gradational with amphibole gneiss to its south and west, and with the Horse Creek foliated granodiorite to the north. In the Horse Creek foliated granodiorite, plagioclase increases to as much as 65 percent and moderately to well-developed foliation is defined by alignment of biotite, lenses of accessory minerals (primarily epidote), or planar zones of differential cataclasis. Passive folds are abundant and some have been refolded to form new passive folds or flexural folds. Granite, aplite, and/or quartz veins occur locally and commonly display pygmatic folds. The biotite gneiss is locally intercalated with amphibole gneiss and is partially equivalent to the quartz-biotite-andesine gneiss unit of Houston and others (1968). Minor quartzite, locally associated with the biotite gneiss, suggests a partial metasedimentary origin for the unit.



Figure 17. Finely layered contorted gneiss.

REFERENCES

- Anonymous, 1896, Albany County, Wyoming, mineral resources: The Laramie Mining and Stock Exchange, Laramie, Wyo., 51 p.
- Beeler, H.C., 1905, Report on the Gold Crater group, Keystone, Albany County, Wyoming: Office of the State Geologist [Wyoming State Geological Survey] Mineral Report 1905-64, 6 p.
- Beeler, H.C., 1906, Mineral and allied resources of Albany County, Wyoming and vicinity: Office of the State Geologist [Wyoming State Geological Survey] Mineral Report MR-1906-82, 79 p.
- Blackstone, D.L., Jr., 1970, Structural geology of the Rex Lake quadrangle, Laramie Basin, Wyoming: Geological Survey of Wyoming [Wyoming State Geological Survey] Preliminary Report 11, 17 p., 1 pl., scale 1:24,000.
- Campbell, E.A., and Shelton, C.R., in press, Preliminary geologic map of the Woods Landing quadrangle, Albany County, Wyoming: Wyoming State Geological Survey Open File Report 2018-3, scale 1:24,000.
- Carnes, J.D., Chumley, A.S., and Samra, C.P., in press, Preliminary geologic map of the Foxpark quadrangle, Albany County, Wyoming: Wyoming State Geological Survey Open File Report 2018-2, scale 1:24,000.
- Coalson, E.B., 1971, Geology of the New Rambler mine area, Albany County, Wyoming: Laramie, University of Wyoming, M.S. thesis, 51 p., 1 pl., scale 1:12,000.
- Currey, D.R., 1965, The Keystone gold-copper prospect area, Albany County, Wyoming: Geological Survey of Wyoming [Wyoming State Geological Survey] Preliminary Report 3, 12 p., 1 pl., approx. scale 1:26,400.
- Dribus, J.B., and Nanna, R.F., 1982, National uranium resource evaluation, Rawlins quadrangle, Wyoming and Colorado: U.S. Department of Energy Report PGJ/F19(82), 116 p., 21 sheets microfiche.
- Ferris, C.S., Jr., and Krueger, H.W., 1964, New radiogenic dates on igneous rocks from the southern Laramie Range, Wyoming: Geological Society of America Bulletin, v. 75, p. 1,051–1,054.
- Frost, C.D., Frost, B.R., Chamberlain, K.R., and Edwards, B.R., 1999, Petrogenesis of the 1.43 Ga Sherman batholith, SE Wyoming, USA—A reduced rapakivi-type anorogenic granite: *Journal of Petrology*, v. 40, no. 12, p. 1,771–1,802.
- Graff, P.J., 1978, Geology of the lower part of the Early Proterozoic Snowy Range Supergroup, Sierra Madre, Wyoming: Laramie, University of Wyoming, Ph.D. dissertation, 85 p.
- Hausel, W.D., 1989, The geology of Wyoming's precious metal lode and placer deposits: Geological Survey of Wyoming [Wyoming State Geological Survey] Bulletin 68, 248 p., 6 pls.
- Hausel, W.D., 1997, Copper, lead, zinc, molybdenum, and associated metal deposits of Wyoming: Wyoming State Geological Survey Bulletin 70, 229 p., 15 pls.
- Hausel, W.D., 2000, The Wyoming platinum-palladium-nickel province: geology and mineralization, in Winter, G.A., editor, *Classical Wyoming geology in the new millenium: Wyoming Geological Association 51st Field Conference Guidebook*, p. 15–27.
- Hills, F.A., Gast, P.W., Houston, R.S. and Swainbank, I.G., 1968, Precambrian geochronology of the Medicine Bow Mountains, southeastern Wyoming: *Geological Society of America Bulletin*, v. 79, no. 12, p. 1,757–1,783.
- Hills, F.A., and Houston, R.S., 1979, Early Proterozoic tectonics of the central Rocky Mountains, North America: *Contributions to Geology*, v. 17, no. 2, p. 89–109.
- Houston, R.S., 1993, Late Archean and Early Proterozoic geology of southeastern Wyoming in Snoke, A.W., Steidtmann, J.R., and Roberts, S.M., eds., *Geology of Wyoming: Geological Survey of Wyoming [Wyoming State Geological Survey] Memoir 5*, v. 1, p. 78–116.

- Houston, R.S., Duebendorfer, E.M., Karlstrom, K.E., and Premo, W.R., 1989, A review of the geology and structure of the Cheyenne belt and Proterozoic rocks of southern Wyoming in Grambling, J.A., and Tewksbury, B.J., eds., Proterozoic geology of the southern Rocky Mountains: Geological Society of America Special Paper 235, p. 1–12.
- Houston, R.S., Karlstrom, K.E., Hills, F.A., and Smithson, S.B., 1979, The Cheyenne belt—A major Precambrian crustal boundary in the western United States [abs]: Geological Society of America Special Paper 11, p. 446.
- Houston, R.S., and McCallum, M.E., 1961, Mullen Creek-Nash Fork shear zone, Medicine Bow Mountains, southeastern Wyoming (abs): Geological Society of America Special Paper 68, p. 91.
- Houston, R.S., McCallum, M.E., and Patchen, A.D., 2003, Geologic map of a portion of the Lake Owen and Albany quadrangles, Albany County, Wyoming, showing major lithologic subdivisions of the Lake Owen mafic complex (unpublished mineral files): Wyoming State Geological Survey, scale 1:24,000.
- Houston, R.S., and Orback, C.J., 1976, Geologic map of the Lake Owen quadrangle, Albany County, Wyoming: U.S. Geological Survey Geologic Quadrangle Map GQ-1304, scale 1:24,000.
- Houston, R.S., and others, 1968, A regional study of Precambrian age in that part of the Medicine Bow Mountains lying in southeastern Wyoming—with a chapter on the relationship between Precambrian and Laramide structure: Geological Survey of Wyoming [Wyoming State Geological Survey] Memoir 1, 167 p., 35 pls., scale 1:63,360, (Reprinted 1978.)
- Houston, R.S., Duebendorfer, E.M., Karlstrom, K.E., and Premo, W.R., 1989, A review of the geology and structure of the Cheyenne belt and Proterozoic rocks of southern Wyoming in Grambling, J.A., and Tewksbury, B.J., eds., Proterozoic geology of the southern Rocky Mountains: Geological Society of America Special Paper 235, p. 1–12.
- Harris, R.E., 1991, Rare earth elements and yttrium in Wyoming (supersedes Geological Survey of Wyoming Open File Report 87-8): Wyoming State Geological Survey Industrial Minerals Report 91-3, 125 p. (Revised, 2002).
- Knight, S.H., 1942, Known mineral resources of Albany County, Wyoming Part I—The metallic minerals: Geological Survey of Wyoming [Wyoming State Geological Survey] unpublished report prepared for the Albany County Counsel of Defense, Mineral Report 42-45, 26 p.
- Lillegraven, J.A., 1993, Correlation of Paleogene strata across Wyoming—A users' guide, in Snoke, A.W., Steidtmann, J.R., and Roberts, S.B., eds., Geology of Wyoming: Geological Survey of Wyoming [Wyoming State Geological Survey] Memoir 5, v. 1, p. 414–477.
- Loucks, R.R., 1976, Platinum-gold-copper mineralization, central Medicine Bow Mountains, Wyoming: Fort Collins, Colorado State University, M.S. thesis, 298 p.
- Loucks, R.R., and Glascock, J.W., 1989, Petrology and PGE mineralization of the early Proterozoic synorogenic Lake Owen layered mafic intrusion, southern Wyoming, USA (unpublished mineral files): Geological Survey of Wyoming [Wyoming State Geological Survey], 39 p., 2 pls., scale 1:12,000.
- Loucks, R.R., Premo, W.R., and Snyder, G.L., 1988, Petrology, structure, and age of the Mullen Creek layered mafic complex and age of arc accretion, Medicine Bow Mountains, Wyoming: Geological Society of America Abstracts with Programs, v. 20, p. A73.
- Love, J.D., 1953, Preliminary report on the uranium deposits in the Miller Hill area, Carbon County, Wyoming: U.S. Geological Survey Circular 278, 10 p., scale 1:63,360.
- Love, J.D., and Christiansen, A.C., comps., 1985, Geologic map of Wyoming: U.S. Geological Survey, 3 sheets, scale 1:500,000, (Re-released 2014, Wyoming State Geological Survey).
- Love, J.D., Christiansen, A.C., and Ver Ploeg, A.J. 1993, Stratigraphic chart showing Phanerozoic nomenclature for the State of Wyoming, Geological Survey of Wyoming [Wyoming State Geological Survey] Map Series 41, 1 sheet.
- Luft, S.J., 1985, Generalized geologic map showing distribution and basal configuration of the Browns Park Formation and Bishop Conglomerate in northwestern Colorado, northeastern Utah, and southern Wyoming: U.S. Geological Survey Miscellaneous Field Studies Map MF-1821, scale 1:250,000.

- McCallum, M.E., 1964, Petrology and structure of the Precambrian and post-Mississippian rocks of the east-central Medicine Bow Mountains, Albany and Carbon counties, Wyoming: Laramie, University of Wyoming, Ph.D. dissertation, 164 p.
- McCallum, M.E., 1968, The Centennial Ridge gold-platinum district, Albany County, Wyoming: Geological Survey of Wyoming [Wyoming State Geological Survey] Preliminary Report 7, 13 p., 1 pl., scale 1:20,000.
- McCallum, M.E., and Houston, R.S., 1985, Geologic map of the Albany quadrangle, Albany County, Wyoming (unpublished mineral files): Geological Survey of Wyoming [Wyoming State Geological Survey], 16 p., 1 pl., scale 1:24,000.
- McCallum, M.E., and Orback, C.J., 1968, The New Rambler copper-gold-platinum district, Albany and Carbon counties, Wyoming: Geological Survey of Wyoming [Wyoming State Geological Survey] Preliminary Report 8, 12 p., 1 pl., scale 1:24,000.
- Montagne, John, 1991, Cenozoic history of the Saratoga Valley area, Wyoming and Colorado: *Contributions to Geology*, v. 29, no. 1, p. 13–70, 1 pl., approx. scale 1:163,510.
- Mussard, D.E., 1982, Petrology and geochemistry of selected Precambrian felsic plutons, southern Medicine Bow Mountains, Wyoming: Fort Collins, Colorado State University, M.S. thesis, 245 p.
- Patchen, A.D., 1987, Petrology and stratigraphy of the Lake Owen layered mafic complex, southeast Wyoming: Laramie, University of Wyoming, M.S. thesis, 163 p., scale 1:24,000.
- Premo, W.R., and Loucks, R.R., 2000, Age and Pb-Sr-Nd isotopic systematics of plutonic rocks from the Green Mountain magmatic arc, southeastern Wyoming: *Rocky Mountain Geology*, v. 35, no. 1, p. 51–70.
- Premo, W.R., and Van Schmus, W.R., 1989, Zircon geochronology of Precambrian rocks in southeastern Wyoming and northern Colorado: in Grambling, J.A., and Tewksbury, B.J., eds., *Proterozoic geology of the Southern Rocky Mountains*: Geological Society of America Special Paper 235, p. 13–32.
- Ramirez, Olivio, 1971, Petrology and structure of the Precambrian metaigneous sequence in the Savage Run Creek area, Carbon County, Wyoming: Fort Collins, Colorado State University, M.S. thesis, 117 p., 1 pl., scale 1:16,000.
- Rocky Mountain Resources Corp., 2007, Lake Owen Project, Albany County, Wyoming, Press Release Oct. 2, 2007, accessed December 2008, at www.rkyresources.com/news/Oct2.pdf.
- Snyder, G.L., 1980, Geologic map of the northernmost Park Range and southernmost Sierra Madre, Jackson and Routt counties, Colorado: U.S. Geological Survey Miscellaneous Investigations Series Map I-1113, scale 1:48,000.
- Strickland, Diana, 2004, Structural and geochronologic evidence for the ca. 1.6 Ga reactivation of the Cheyenne belt, southeastern Wyoming: Laramie, University of Wyoming, M.S. thesis, 151 p.
- Sullivan, W.A., and Beane, R.J., 2013, A new view of an old suture—Evidence for sinistral transpression in the Cheyenne belt: *Geological Society of American Bulletin*, v. 125, no. 7–8, p. 1,319.
- Sutherland, W.M., and Cola, E.C., 2016, A comprehensive report on rare earth elements in Wyoming: Wyoming State Geological Survey Report of Investigations 71, 137 p.
- Sutherland, W.M., Durnan, J.A., and Johnson, J.F., 2013, Preliminary geologic map of the Centennial quadrangle, Albany County, Wyoming: Wyoming State Geological Survey Open File Report 13-5, scale 1:24,000.
- Sutherland, W.M., and Hausel, W.D., 1999, Mineral Resource Survey of the Medicine Bow National Forest (unpublished mineral files): Wyoming State Geological Survey, 3 p., 56 pls., scale 1:24,000.
- Sutherland, W.M., and Hausel, W.D., 2005a, Preliminary geologic map of the Saratoga 30° x 60° quadrangle: Wyoming State Geological Survey Open File Report 04-10, 34 p., 1 pl., scale 1:100,000.
- Sutherland, W.M., and Hausel, W.D., 2005b, Preliminary geologic map of the Keystone quadrangle, Albany and Carbon counties, Wyoming: Wyoming State Geological Survey Open File Report 05-6, 21 p., scale 1:24,000.

- Swetnam, M.N., 1961, Geology of the Pelton Creek area, Albany and Carbon counties, Wyoming: Laramie, University of Wyoming, M.S. thesis, 78 p., 1 pl., scale 1:15,500.
- Ver Ploeg, A.J., Larsen, M.C., and Taboga, K.G., 2016, Characterization of evaporite karst features in the southern Laramie Basin, Wyoming: Wyoming State Geological Survey Report of Investigations 70, 34 p.
- Vine, J.D., and Prichard, G.E., 1959, Geology and uranium occurrences in the Miller Hill area, Carbon County, Wyoming: U.S. Geological Survey Bulletin 1074-F, 239 p., 7 pls., scale 1:48,000.

Appendices

APPENDIX I: SAMPLE DESCRIPTIONS AND LOCATIONS

Table A–1. Albany quadrangle samples taken January 9, 2018.

Sample Number	Sample Description	WGS-84	
		Lat.	Long.
20170615WS-A	clean Keystone Quartz Diorite - Xk	41.175	-106.241
20170710NK-B	silicified pumice or tufa; float	41.155	-106.136
20170710NK-F	LO olivine magnetite gabbro-norite - Xlu	41.156	-106.132
20170710NK-I	clean Sherman Granite - Ys	41.186	-106.164
20170710NK-J	adit in altered Fe- & Cu-stained older granite (Xg) near LO xenolith	41.185	-106.143
20170711NK-B2	LO gabbro-norite (Xlgn): may be troctolite within gabbro-norite layer; no nodular weathering	41.156	-106.166
20170718NK-D	LO sheared/brecciated, red-stained gabbro within magnetite gabbro layer (Xlm)	41.132	-106.146
20170719NK-C	zoned pegmatite (YXp) in contact with LO gabbro	41.150	-106.188
20170719NK-F2	mylonitic felsic gneiss - Xv	41.135	-106.205
20170720NK-C	prospect pit in Browns Park Fm dirty limestones/lvs breccia (Tl); probable hot spring tufa	41.150	-106.204
20170725NK-A	LO basal unit (Xlb) metabasalt & breccia at contact with andesine gneiss (Xv)	41.132	-106.186
20170725NK-C	Browns Park Fm limestone/lvs breccia (Tl) with felsic clasts; probable hot spring tufa; (N pit)	41.131	-106.186
20170803NK-A	felsic dike (Xgf) cutting LO norite (Xln)	41.185	-106.150
20170803NK-I	Keystone quartz diorite transition zone - Xki	41.171	-106.226
20170803NK-K	small (not mapped) felsic dike cutting Xki	41.176	-106.223
20170804NK-A	Fe-stained qtz vein cutting sheared Xki; Lucky Luke prospect pit	41.159	-106.225
20170804NK-B	quartzo-feld gneiss (Xvf) near prospect & contact with Xvf to S.	41.158	-106.226
20170809NK-B	v fine-grain, pink-weathering, 20 ft wide, mafic dike cutting Xk; andesite (Xsan)	41.175	-106.235
20170809NK-F	4 prospect pits in Fe-stained qtz vein cutting Xk along fault/SZ	41.170	-106.245
20170809NK-H	Horse Creek foliated granodiorite (Xgh); contorted	41.210	-106.229
20170810NK-E	collapsed shaft in Xk; Fe-stained, vuggy to punky & massive bull qtz; minor sulfides, malachite, Cu-sulfides	41.173	-106.248
20170811NK-A	shaft & open adit in contorted gneiss (Xcbg); Fe-stained qtzite, epidote; fine grained mafics & felsics, breccias	41.177	-106.250
20170811NK-E	Epidote [Radiometric date sample]; collapsed adit in quartz-biotite gneiss (Xqb); epidotized gneiss, minor schist, SZ, Fe-stain, sulfides (?)	41.187	-106.233
20170824NK-F	Cuprite mine epidote; adit in very fine grained mafic dike cutting Xhg; abundant Kspar, epidote, small quartz veins; massive calcite veins cut all else (emplaced last)	41.198	-106.241
20170824NK-G	Cuprite mine calcite; adit in very fine grained mafic dike cutting Xhg; abundant Kspar, epidote, small quartz veins; massive calcite veins cut all else (emplaced last)	41.198	-106.241
20170825NK-A	Adit & shaft in Xk on Florence trend: Fe-stained quartz, breccia, fault gouge, epidote	41.165	-106.249
20170825NK-F1	Dump sample from inclined water-filled shaft in Xk: Fe-stained calcite	41.163	-106.246
20170825NK-F2	Dump sample from inclined water-filled shaft in Xk: qtz, limonite, epidote, breccia	41.163	-106.246

Table A-1 continued.

20170825NK-I	mylonitic gneiss (Xmy) with epidote; both mafic & felsic	41.222	-106.218
20170912NK-H	Andesite dike - Xsan [Radiometric date sample]	41.174	-106.231
20170921NK-A	Lake Owen layered unit (XII), layered gabbro-norite with sulfides [Radiometric date sample]	41.185	-106.157

APPENDIX 2: WHOLE ROCK CHEMICAL ANALYSES

Table A-2. Albany quadrangle whole rock analyses.

Sample Number	SiO ₂ %	Al ₂ O ₃ %	Fe ₂ O ₃ %	CaO %	MgO %	Na ₂ O %	K ₂ O %	Cr ₂ O ₃ %	TiO ₂ %	MnO %	P ₂ O ₅ %	SiO %	BaO %	C %	S %	LOI %	Total %
20170615WS-A	62	16.7	6.89	5.7	2.67	3.72	1.85	0.01	0.64	0.12	0.2	0.07	0.08	0.01	0.02	0.94	101.59
20170710NK-B	91.5	0.97	3.95	0.24	0.5	0.09	0.09	0.01	0.03	0.34	0.04	<0.01	0.03	0.2	0.01	3.69	101.48
20170710NK-F	47.6	17.25	10.8	10.75	10.8	2.13	0.11	0.06	0.1	0.17	0.01	0.09	0.01	0.13	0.03	0.15	100.03
20170710NK-I	71.4	13.3	4.13	1.44	0.44	3.39	4.79	<0.01	0.36	0.07	0.07	0.02	0.12	0.02	<0.01	0.81	100.34
20170710NK-J	8.62	1.09	72.5	1.16	1.97	0.07	0.04	0.17	7.79	0.69	0.04	<0.01	0.11	0.11	0.09	5.08	99.33
20170711NK-B2	46.6	22.2	6.17	13.4	8.14	1.63	0.07	0.05	0.1	0.1	0.01	0.07	0.01	0.03	0.01	0.81	99.36
20170718NK-D	46.7	16.7	13.4	12.65	5.64	2.46	0.11	0.01	1.1	0.16	0.01	0.09	0.01	0.02	0.01	0.21	99.25
20170719NK-C	73.9	14.2	1.89	0.59	0.15	5.38	1.35	<0.01	0.03	1.15	0.02	<0.01	<0.01	0.03	<0.01	0.52	99.18
20170719NK-F2	72.5	15.1	1.37	3.52	0.3	4.35	1.85	<0.01	0.32	0.04	0.08	0.05	0.1	0.12	<0.01	0.59	100.17
20170720NK-C	9.28	3.2	1.38	46.9	1.06	1	0.39	<0.01	0.11	0.02	0.08	0.02	0.03	9.63	0.02	37.2	100.67
20170725NK-A	44.5	8.96	11.5	9.03	19.7	0.41	0.15	0.23	0.29	0.2	0.09	0.01	<0.01	0.09	<0.01	5.04	100.11
20170725NK-C	17.8	5.42	2.92	39.2	0.79	2.31	0.33	<0.01	0.33	0.06	0.14	0.02	0.01	7.9	0.02	31.2	100.53
20170803NK-A	73.3	12.9	2.36	1.45	0.56	2.46	5.1	0.01	0.28	0.04	0.04	0.04	0.25	0.07	<0.01	0.88	99.67
20170803NK-I	76.2	12.95	1.74	1.16	0.28	2.48	5.72	<0.01	0.16	0.03	0.04	0.02	0.1	0.05	<0.01	0.63	101.51
20170803NK-K	76.7	12.4	1.95	1.05	0.37	2.43	5.35	<0.01	0.2	0.03	0.06	0.03	0.27	0.13	<0.01	0.76	101.6
20170804NK-A	99.3	0.09	1.81	0.04	0.01	0.02	0.02	0.01	<0.01	0.01	0.02	<0.01	<0.01	0.03	0.01	0.35	101.68
20170804NK-B	73.8	13.7	2.66	0.99	0.18	3.65	4.24	<0.01	0.16	0.06	0.05	0.02	0.06	0.02	<0.01	0.69	100.26
20170809NK-B	61	15	9.97	3.88	1.17	3.6	2.9	<0.01	1.05	0.13	0.48	0.06	0.2	0.09	0.01	1.47	100.91
20170809NK-F	78.9	2.32	14.7	0.07	0.09	0.18	1.08	0.01	0.02	0.01	0.05	<0.01	0.07	0.07	0.01	3.11	100.61
20170809NK-H	72.3	14.45	2.62	2.07	0.59	4.02	3.56	0.01	0.22	0.06	0.07	0.05	0.12	0.02	<0.01	0.57	100.71
20170810NK-E	82.1	6.79	5.08	0.29	0.73	1.33	1.31	0.01	0.34	0.04	0.14	0.01	0.06	0.06	0.22	1.91	100.14
20170811NK-A	89.1	1.39	5.75	1.48	0.21	0.25	0.09	<0.01	0.05	0.04	0.02	<0.01	<0.01	0.04	0.04	0.76	99.14
20170811NK-E	53.1	14.5	10.7	16.25	2.61	0.12	0.04	0.02	0.68	0.26	0.16	0.02	0.01	0.05	0.01	1.83	100.3
20170824NK-F	47.7	8.77	12.2	13.5	12.6	0.82	0.55	0.12	0.6	0.27	0.2	0.1	0.01	0.02	<0.01	2.14	99.58
20170824NK-G	31.3	1.46	0.93	38.3	0.35	0.25	0.46	0.01	0.03	0.18	0.03	0.02	0.01	7.64	0.01	28.4	101.73
20170825NK-A	33.7	2.51	7.57	23.7	4.77	0.25	0.55	<0.01	0.11	0.66	0.04	0.02	0.03	7.26	0.01	25	98.91
20170825NK-F1	9.03	2.06	5.4	42.5	2.46	0.07	0.33	0.02	0.04	0.5	0.02	0.02	0.02	9.85	0.02	36.9	99.37
20170825NK-F2	37.6	10.4	8.17	22	3.12	1.32	0.58	0.04	0.47	0.28	0.16	0.05	0.03	3.81	0.01	16.35	100.57
20170825NK-I	72.4	14.3	2.88	1.25	0.44	4.43	4.28	<0.01	0.28	0.03	0.05	0.02	0.13	0.08	<0.01	1.02	101.51
20170912NK-H	60.2	15.15	9.91	4.16	1.28	3.66	2.93	<0.01	1.05	0.2	0.45	0.06	0.2	0.07	0.02	1.11	100.36
20170921NK-A	52	17.4	5.8	11.45	7.55	2.47	0.61	0.02	0.19	0.12	0.03	0.08	0.02	0.05	0.06	2.25	99.99

APPENDIX 3: ALBANY QUADRANGLE TRACE ELEMENT CHEMICAL ANALYSES

Table A-3. Albany quadrangle trace element chemical analyses.

Sample Number	ME-4ACD81 Ag ppm	ME-MS42 As ppm	Au-AA25 Au ppm	PGM-ICP24 Au ppm	ME-MS81 Ba ppm	ME-MS42 Bi ppm	ME-4ACD81 Cd ppm	ME-MS81 Ce ppm	ME-4ACD81 Co ppm	ME-MS81 Cr ppm	ME-MS81 Cs ppm	ME-4ACD81 Cu ppm	ME-MS81 Dy ppm	ME-MS81 Er ppm
20170615WS-A	<0.5	8.4	0.01		709	3.66	<0.5	47.7	16	50	1.86	56	3.45	2.13
20170710NK-B	<0.5	9.9	0.01		249	0.43	<0.5	23.1	36	40	0.43	43	0.45	0.29
20170710NK-F	<0.5	1.6	0.01	0.006	87.6	0.11	<0.5	2.6	67	410	0.09	91	0.47	0.25
20170710NK-I	<0.5	2.1			1050	0.09	<0.5	164	4	20	2.51	8	10.7	6.38
20170710NK-J	<0.5	28.2	0.02	0.005	930	0.8	2.4	5	49	1300	0.86	736	0.3	0.19
20170711NK-B2	<0.5	0.9	0.01	<0.001	53.5	0.03	<0.5	2.5	38	380	0.08	56	0.44	0.33
20170718NK-D	<0.5	0.3	0.01	0.005	78.7	0.02	<0.5	3.7	29	60	0.04	113	0.98	0.47
20170719NK-C	<0.5	2.5	<0.01	<0.001	19.2	0.18	<0.5	89.7	1	30	4.63	8	37.7	22.2
20170719NK-F2	<0.5	3			956	0.12	<0.5	16.7	2	30	0.41	38	0.74	0.49
20170720NK-C	<0.5	7.7	0.01		249	0.1	<0.5	11.2	3	30	1.01	42	0.74	0.55
20170725NK-A	<0.5	8.5	<0.01	<0.001	25.9	0.02	<0.5	13.1	69	1730	0.06	65	1.87	1.28
20170725NK-C	<0.5	11	0.02		88.7	0.02	<0.5	14.5	3	40	0.5	47	1.95	1.31
20170803NK-A	<0.5	2.8			2230	0.05	<0.5	29.3	4	40	2.12	6	1.45	0.88
20170803NK-I	<0.5	1.8			886	0.02	<0.5	44.2	2	30	0.56	19	1.24	0.62
20170803NK-K	<0.5	1.9			2380	0.02	<0.5	22.7	3	20	0.46	25	1.04	0.63
20170804NK-A	<0.5	4.4	0.01		8.6	0.01	<0.5	0.7	2	50	0.04	190	<0.05	<0.03
20170804NK-B	<0.5	1.6	<0.01		485	0.01	<0.5	59.7	1	30	0.88	11	2.82	2.26
20170809NK-B	<0.5	7.5	0.01	<0.001	1745	0.08	<0.5	36.8	7	30	3.15	13	6.2	3.74
20170809NK-F	1.3	249	0.18		618	3.17	<0.5	4.3	163	50	0.46	800	0.82	0.51
20170809NK-H	<0.5	1.3			1090	0.09	<0.5	54	4	40	0.71	8	1.54	0.89
20170810NK-E	16.3	36.6	72.2		492	>250	<0.5	13	25	40	0.75	7720	1.38	0.86
20170811NK-A	0.8	7.9	0.01		37.3	0.68	<0.5	10.5	2	30	0.11	144	0.47	0.39
20170811NK-E	<0.5	13.5	0.01	0.001	47.6	0.24	<0.5	33.4	33	170	0.28	144	3.89	2.21
20170824NK-F	<0.5	4.3	0.08		97.6	0.89	<0.5	72.6	44	910	0.09	31	2.85	1.42
20170824NK-G	<0.5	1.5	0.01		83.2	0.1	<0.5	12.6	1	60	0.21	12	2.24	2.14
20170825NK-A	<0.5	3.8	<0.01	0.001	256	0.03	<0.5	39.6	7	10	0.3	6	7.02	4.45
20170825NK-F1	<0.5	4.9			152.5	0.06	<0.5	38.9	5	130	0.14	5	8.3	4.93
20170825NK-F2	<0.5	5.6	0.02		238	0.08	<0.5	41.2	10	260	0.18	12	4.82	2.59
20170825NK-I	<0.5	2.2			1130	0.33	<0.5	49.2	3	40	0.42	26	4.17	2.68
20170912NK-H	<0.5	1.6	<0.01	<0.001	1810	0.04	<0.5	94.3	12	<10	2.62	18	6.92	4.25
20170921NK-A	<0.5	3.2	<0.01	0.004	181	0.06	<0.5	4.2	31	160	2.21	220	0.78	0.58

Table A-3 continued.

Sample Number	ME-MS81 ppm	Eu ppm	ME-MS81 ppm	Ga ppm	ME-MS81 ppm	Gd ppm	ME-MS81 ppm	Ge ppm	Hf ppm	ME-MS42 ppm	Hg ppm	ME-MS81 ppm	Ho ppm	In ppm	ME-MS42 ppm	La ppm	Li ppm	ME-MS81 ppm	Lu ppm	Mo ppm	ME-MS81 ppm	Nb ppm	ME-MS81 ppm	Nd ppm
20170615WS-A	1.07	17.7	3.86	<5	4.2	0.01	0.71	0.012	22	20	0.3	<1	10	24.5										
20170710NK-B	0.15	1.5	0.54	<5	0.3	0.018	0.08	<0.005	5.4	<10	0.02	2	1.6	4.9										
20170710NK-F	0.33	12.4	0.35	<5	<0.2	0.012	0.07	<0.005	1.3	<10	0.03	<1	0.4	1.7										
20170710NK-I	1.64	22.2	10.95	<5	11.2	0.006	2.25	0.053	82.4	20	0.87	<1	22.1	69.5										
20170710NK-J	0.15	30.1	0.4	<5	0.4	0.015	0.08	0.023	4.3	<10	0.03	61	4.1	3.1										
20170711NK-B2	0.21	12.6	0.36	<5	<0.2	0.006	0.06	<0.005	1.2	<10	0.04	<1	0.2	1.5										
20170718NK-D	0.51	19	1.09	<5	0.7	<0.005	0.19	0.008	1.5	10	0.08	<1	0.4	3										
20170719NK-C	0.13	36.2	24	5	18.4	<0.005	7.75	0.005	31.9	10	3.86	<1	110.5	59.6										
20170719NK-F2	0.54	16.5	0.67	<5	5.6	<0.005	0.16	0.005	11.9	<10	0.12	1	4.9	5										
20170720NK-C	0.28	4.7	0.91	<5	1	0.028	0.18	0.009	10	20	0.07	<1	2	7										
20170725NK-A	0.47	9.6	1.7	<5	1	<0.005	0.41	0.009	6.1	30	0.2	<1	2.1	7.6										
20170725NK-C	1.55	7	2.65	<5	0.6	0.021	0.49	0.018	10.1	10	0.21	<1	3.6	13.2										
20170803NK-A	0.66	13.3	1.58	<5	5.9	<0.005	0.33	<0.005	13.7	10	0.21	<1	9.4	11										
20170803NK-I	0.45	12.8	1.63	<5	4	<0.005	0.27	<0.005	25.4	<10	0.09	1	2.4	16.9										
20170803NK-K	0.48	11	1.17	<5	2.7	0.006	0.18	<0.005	14.1	10	0.08	1	3	10.3										
20170804NK-A	<0.03	0.3	0.07	<5	<0.2	<0.005	0.01	0.025	0.8	<10	<0.01	2	<0.2	0.5										
20170804NK-B	0.45	19.5	2.08	<5	5.6	<0.005	0.73	0.009	11.4	10	0.53	<1	19.3	10.9										
20170809NK-B	2.18	22.2	6.14	<5	6	0.005	1.36	0.025	17.4	20	0.54	1	17	23.3										
20170809NK-F	0.2	2.8	0.87	<5	<0.2	0.011	0.17	0.073	5	<10	0.06	2220	0.2	5										
20170809NK-H	0.61	16.7	1.7	<5	4.1	<0.005	0.34	0.005	24.8	20	0.15	11	6.9	15.2										
20170810NK-E	0.41	9.5	1.43	<5	2	0.471	0.3	0.115	6.7	10	0.16	14	4.8	6.9										
20170811NK-A	0.11	3.1	0.47	<5	0.5	0.012	0.1	0.023	7.7	<10	0.07	4	0.7	3.3										
20170811NK-E	1.26	18.6	4.05	<5	2.4	0.011	0.79	0.02	16.2	<10	0.31	5	5.3	17.3										
20170824NK-F	1.59	13.7	4.72	<5	1.5	0.006	0.56	0.021	31	10	0.21	1	8.4	39.7										
20170824NK-G	0.43	1.9	2.22	<5	<0.2	<0.005	0.68	0.039	7.7	<10	0.61	1	0.3	6.9										
20170825NK-A	2.03	4.2	6.76	<5	0.7	0.006	1.53	0.065	20.1	10	0.61	<1	1	23.9										
20170825NK-F1	2.32	4.5	7.38	<5	0.2	0.006	1.8	0.104	23.9	10	0.75	9	0.3	24.2										
20170825NK-F2	1.94	17	5.1	<5	1.5	0.007	1.03	0.05	24.4	20	0.43	2	4.4	23.8										
20170825NK-I	0.68	17.8	3.73	<5	8.7	<0.005	0.98	0.028	18.6	10	0.5	3	16	19.1										
20170912NK-H	3.01	22	8.13	<5	5.6	<0.005	1.45	0.015	38.6	20	0.57	1	16.3	44										
20170921NK-A	0.41	14.1	0.92	<5	0.2	0.04	0.2	<0.005	1.8	20	0.08	1	0.4	3										

Table A-3 continued.

Sample Number	ME-4ACD81 Ni ppm	ME-4ACD81 Pb ppm	PGM-ICP24 Pd ppm	PGM-ICP24 Pr ppm	ME-MS81 Pt ppm	PGM-ICP24 Rb ppm	ME-MS81 Re ppm	ME-MS42 Sb ppm	ME-4ACD81 Sc ppm	ME-MS42 Se ppm	ME-MS81 Sm ppm	ME-MS81 Sn ppm	ME-MS81 Sr ppm	ME-MS81 Ta ppm
20170615WS-A	17	6		6		45	<0.001	0.86	15	<0.2	4.52	1	669	0.5
20170710NK-B	15	7		1.22		3.9	<0.001	0.48	1	0.5	0.78	<1	28.3	0.1
20170710NK-F	235	<2	0.036	0.32	0.013	1.4	<0.001	0.77	22	0.2	0.4	<1	769	<0.1
20170710NK-I	3	22		18		154.5	<0.001	0.22	5	<0.2	12.45	4	140	1.4
20170710NK-J	216	354	0.306	0.81	0.28	2.3	0.009	0.33	19	12.4	0.44	3	20	0.1
20170711NK-B2	252	<2	0.035	0.35	0.014	1	<0.001	0.09	13	<0.2	0.4	<1	594	<0.1
20170718NK-D	33	<2	0.001	0.59	<0.005	0.9	<0.001	0.05	45	0.3	0.85	1	740	0.1
20170719NK-C	1	21	<0.001	12.9	<0.005	169	<0.001	0.14	10	<0.2	22.3	13	33.5	16.9
20170719NK-F2	1	9		1.53		29.9	<0.001	0.33	5	<0.2	0.86	1	453	0.3
20170720NK-C	4	2		1.67		9.5	<0.001	0.21	3	0.3	1.06	<1	152.5	0.1
20170725NK-A	755	<2	0.004	1.77	0.008	1.8	<0.001	0.22	22	0.2	1.68	1	67.6	0.1
20170725NK-C	9	2		2.5		8.7	<0.001	0.27	7	0.5	2.7	<1	147	0.1
20170803NK-A	8	14		3.06		114.5	<0.001	0.14	2	<0.2	2.03	1	311	0.7
20170803NK-I	11	19		4.85		82.5	<0.001	0.11	3	<0.2	2.57	<1	163	0.1
20170803NK-K	2	12		2.92		72.3	<0.001	0.13	1	<0.2	1.68	1	275	0.1
20170804NK-A	1	<2		0.13		0.5	<0.001	0.16	<1	<0.2	0.09	<1	4.1	<0.1
20170804NK-B	2	19		3.14		132.5	<0.001	0.09	2	<0.2	2.43	5	144	1.4
20170809NK-B	<1	17	<0.001	5.17	<0.005	77	<0.001	0.31	20	<0.2	6.1	2	532	0.9
20170809NK-F	53	48		1.26		11	0.203	1.33	<1	4	0.94	<1	31.8	<0.1
20170809NK-H	2	12		4.3		91.2	<0.001	0.08	3	<0.2	2.28	1	401	0.5
20170810NK-E	26	8		1.7		28.9	0.001	0.7	8	0.9	1.39	1	80.4	0.2
20170811NK-A	4	234		1.07		2.2	<0.001	0.43	1	1.5	0.47	1	34.3	0.1
20170811NK-E	42	10	0.002	4.2	<0.005	2.1	<0.001	2.53	25	0.3	3.98	2	188.5	0.3
20170824NK-F	214	11		9.54		10.8	<0.001	0.43	41	<0.2	6.11	1	80.4	0.2
20170824NK-G	2	4		1.58		13.4	<0.001	0.08	9	0.4	1.35	<1	167	<0.1
20170825NK-A	5	3	<0.001	5.32	<0.005	10.1	<0.001	0.18	10	<0.2	5.99	1	230	0.1
20170825NK-F1	22	9		5.11		6.5	<0.001	0.17	15	0.2	6.14	1	175.5	<0.1
20170825NK-F2	48	8		5.5		11.8	<0.001	0.26	20	0.3	5.4	2	423	0.1
20170825NK-I	5	15		4.83		84.4	<0.001	0.2	6	<0.2	3.99	3	132	1
20170912NK-H	1	18	<0.001	11.15	<0.005	71.1	<0.001	0.15	21	<0.2	8.98	2	540	1.1
20170921NK-A	109	3	0.003	0.6	0.012	28.1	<0.001	0.15	35	0.4	0.82	<1	707	<0.1

APPENDIX 4: RADIOMETRIC DATING OF SAMPLES FROM WITHIN THE ALBANY QUADRANGLE

Report submitted to the Wyoming State Geological Survey on CATIMS U-Pb zircon dating of Lake Owen mafic complex in the Albany Quadrangle

April 12, 2018. Kevin R. Chamberlain, Research Professor, Dept. of Geology and Geophysics, University of Wyoming

Summary

20170921NK-A Lake Owen complex: 1775.1 \pm 3.0 Ma (Concordia Age from 4 points, 95% confidence) from a layered gabbro-norite from the layered unit (XII). Improves the precision on previously published Nd isochron date of 1750 \pm 24 Ma (Premo and Loucks 2000).

Methods

Zircon grains were separated by standard crushing and mineral separation methods. Selected zircons were annealed at 850 °C for 50 hours, then dissolved in two steps in a chemical abrasion, thermal ionization mass spectrometric U-Pb dating method (CA-TIMS) modified from Mattinson (2005). The first dissolution step was in hydrofluoric acid (HF) and nitric acid (HNO₃) at 180 °C for 12 hours. This removed the most metamict zircon domains in the annealed crystals. Individual grains were then spiked with a mixed ²⁰⁵Pb-²³³U-²³⁵U tracer (ET535), completely dissolved in HF and HNO₃ at 240 °C for 30 hours, and then converted to chlorides. The dissolutions were loaded onto rhenium filaments with phosphoric acid and silica gel without any further chemical processing. Pb and UO₂ isotopic compositions were determined in single Daly-photomultiplier mode on a Micromass Sector 54 mass spectrometer. Data were reduced and ages calculated using PbMacDat and ISOPLOT/EX after Ludwig (1988, 1991, 1998). The Concordia Age used in this report is a specific algorithm created by Ludwig (1998) to combine both ²⁰⁶Pb/²³⁸U and ²⁰⁷Pb/²³⁵U data from concordant analyses. Concordia Ages reported here include the contributions from the U-decay constant uncertainties and can be compared to dates from other methods as long as those methods also propagate all sources of uncertainty.

Results

20170921NK-A Lake Owen complex. This sample is layered gabbro-norite from the layered unit (XII), that is coarse grained and pegmatitic and showed up to ~80 ppm Zr with in-house XRF measurement. Zircons recovered from this sample were relatively large (some >400 microns) with varied anhedral shapes (Figure 1). These morphologies are typical of magmatic zircons in mafic to gabbroic rocks (e.g. Krogh et al., 1987; Scoates and Chamberlain 1995; Doughty and Chamberlain 1996) and are interpreted to reflect magmatic growth in the Lake Owen complex. Four single, analyzed zircons overlap each other on concordia and yield a Concordia Age (Ludwig 1998) of 1775.1 \pm 3.0 Ma (95% confidence, Figure 2); the 2 sigma uncertainty on this date is \pm 1.8 Ma. The Concordia Age includes the uncertainties of the uranium decay constants and is interpreted as the best estimate of the magmatic age of this intrusion. These results agree with published date of 1750 \pm 24 Ma (Premo and Loucks 2000), but improve both the precision and confidence in the age, as the published date was based on Nd isotopic data from mineral separates.

This new date for the Lake Owen also strengthens potential correlations with nearby mafic plutons in the Medicine Bow Mountains (Mullen mafic complex zircon date of 1776 \pm 2 Ma, Premo and Loucks 2000), and northern Park Range (Elkhorn Mountain gabbro, 1774-1770 Ma from syn-magmatic and crosscutting dikes, Pallister and Aleinikoff 1987). The higher precision of the new date also establishes that the Lake Owen complex is associated with early arc magmatism, ca. 1.78 Ga (Premo et al., 1989) rather than post-accretion rifting ca. 1.76 Ga (Scoates and Chamberlain 1997; Jones et al., 2010) or post-tectonic magmatism ca. 1.74 Ga (Chamberlain 1998; Jones et al., 2010).

References (including Tables 1):

- Chamberlain, K.R., 1998, Medicine Bow Orogeny: Timing of deformation and model of crustal structure produced during continent-arc collision, ca. 1.78 Ga, southeastern Wyoming: *Rocky Mountain Geology*, v. 33, no. 2, p. 259-278.
- Doughty, P.T., and Chamberlain, K.R., 1996, Salmon River Arch revisited: new evidence for rifting in the Mid-Proterozoic Belt-Purcell basin: *Canadian Journal of Earth Sciences*: v. 33, p. 1037-1052.
- Jones, D.S., Snoke, A.W., Premo, W.R., and Chamberlain, K.R., 2010, New models for Paleoproterozoic orogenesis in the Cheyenne belt region: Evidence from the geology and U-Pb geochronology of the Big Creek Gneiss, southeastern Wyoming. *GSA Bulletin*, v. 122; no. 11-12; p. 1877-1898. doi:10.1130/B30164.1
- Krogh, T.E., 1973, A low-contamination method for hydrothermal decomposition of zircon and extraction of U and Pb for isotopic age determinations: *Geochimica et Cosmochimica Acta*, v. 37, p. 485–494.
- Krogh, T.E., Corfu, F., Davis, D.W., Dunning, G.R., Heaman, L.M., Kamo, S.L., Machado, N., Greenough, J.D., and Nakamura, E. 1987. Precise U-Pb isotopic ages of diabase dykes and mafic to ultramafic rocks using trace amounts of baddeleyite and zircon. In *Mafic dyke swarms*. Edited by H.C. Halls and W.F. Fahrig, Geological Association of Canada, Special paper 34, pg 147-152.
- Ludwig, K.R., 1988, PBDAT for MS-DOS, a computer program for IBM-PC compatibles for processing raw Pb-U-Th isotope data, version 1.24: U.S. Geological Survey, Open-File Report 88-542, 32 pp.
- Ludwig, K.R., 1991, ISOPLOT for MS-DOS, a plotting and regression program for radiogenic-isotope data, for IBM-PC compatible computers, version 2.75: U.S. Geological Survey, Open-File Report 91-445, 45 pp.
- Ludwig, K. R., 1998, On the treatment of concordant uranium-lead ages. *Geochimica et Cosmochimica Acta*, 62(4), 665-676.
- Mattinson, J.M, 2005, Zircon U-Pb chemical abrasion (“CA-TIMS”) method: combined annealing and multi-step partial dissolution analysis for improved precision and accuracy of zircon ages: *Chemical Geology*, v. 220, p. 47-66.
- Pallister, J.S. and Aleinikoff, J.N., 1987, Gabbroic plutons south of the Cheyenne belt: underpinnings of an Early Proterozoic continental margin arc. *Geological Society of America Abstracts with Programs*, v. 19, no. 5, p. 325.
- Parrish, R.R., Roddick, J.C., Loveridge, W.D., and Sullivan, R.D., 1987, Uranium-lead analytical techniques at the geochronology laboratory, Geological Survey of Canada, *in* Radiogenic age and isotopic studies, Report 1: Geological Survey of Canada Paper 87-2, p. 3–7.
- Premo, W.R. and Loucks, R.R., 2000. Age and Pb-Sr-Nd isotopic systematics of plutonic rocks from the Green Mountain magmatic arc, southeastern Wyoming: Isotopic characterization of a Paleoproterozoic island arc system. *Rocky Mountain Geology*, 35(1), pp.51-70.
- Premo, W.R. and Van Schmus, W.R., 1989. Zircon geochronology of Precambrian rocks in southeastern Wyoming and northern Colorado in Grambling, J.A. and Tewksbury, B.J., eds. *Proterozoic Geology of the Southern Rocky Mountains: Geological Society of America Special Paper*, 235, pp.13-32.
- Scoates, J.S. and Chamberlain, K.R., 1995, Baddeleyite (ZrO₂) and zircon (ZrSiO₄) from anorthositic rocks of the Laramie Anorthosite complex, Wyoming: Petrologic consequences and U-Pb ages: *American Mineralogist*, v. 80, p. 1319-1329.

Scoates, J.S. and Chamberlain, K.R., 1997, Orogenic to Post-orogenic origin for the 1.76 Ga Horse Creek anorthosite complex, Wyoming, USA: *Journal of Geology*, v. 105, p. 331-343.

Stacey, J.S. and Kramers, J.D., 1975, Approximation of terrestrial lead isotope evolution by a two-stage model: *Earth and Planetary Science Letters*, v. 26, p. 207-221.

Steiger, R.H. and Jäger, E., 1977, Subcommittee on geochronology: convention on the use of decay constants in geo- and cosmochronology: *Earth and Planetary Science Letters*, v. 36, p. 359-362.



Figure 1. Examples of extra large, anhedral zircons from a layered gabbro-norite in the Lake Owen mafic complex, sample 20170921 NK-A. The anhedral shapes support an interpretation of magmatic growth for these zircons; inherited grains would tend to be more euhedral and embayed. The zircons shown probably grew interstitially late in the crystallization of the complex.

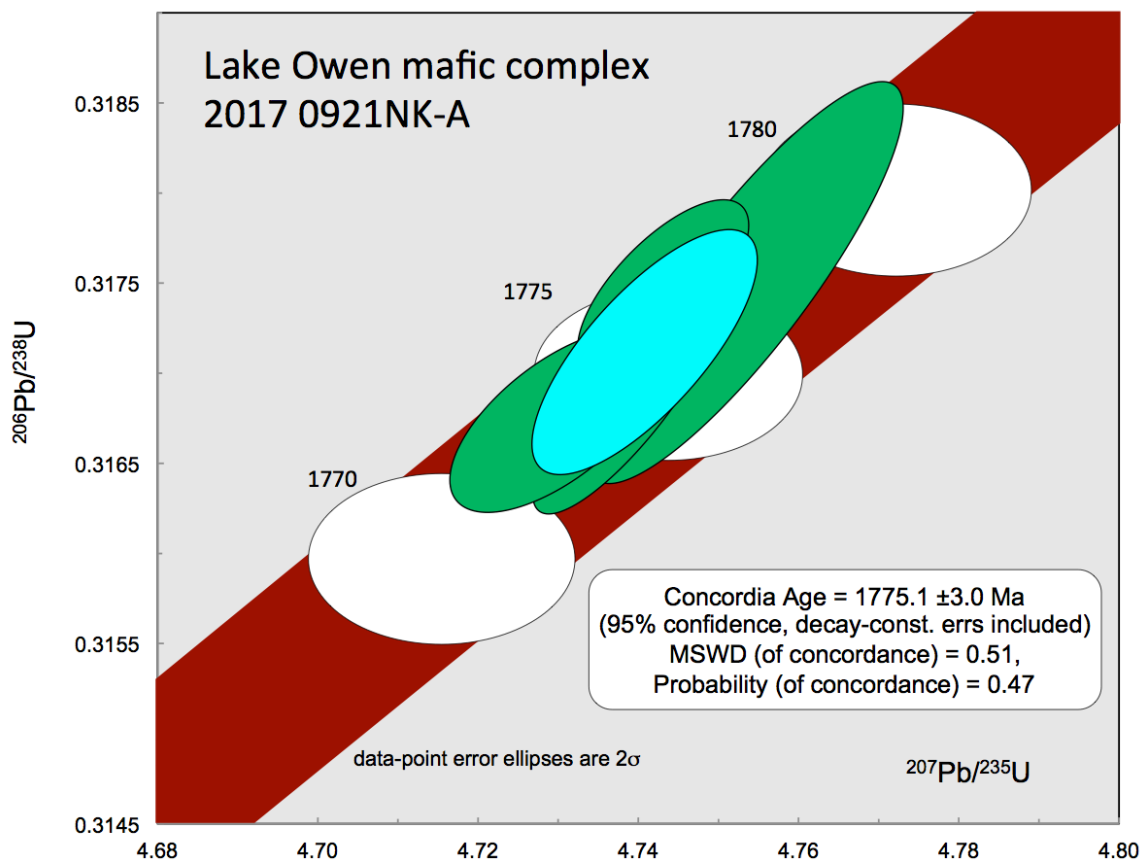


Figure 2. Concordia plot of 4 single zircon CATIMS analyses from 20170921NK-A, a sample of layered gabbro-norite from the Lake Owen mafic complex in the Albany quadrangle, SE Wyoming. Uncertainties in the U-decay constants are shown as a swath for the concordia curve. The 4 green ellipses overlap each other and concordia and yielded a Concordia Age of 1775.1±3.0 Ma (95% confid., ±1.8 at 2 sigma interval).

Table 1 CATIMS U-Pb zircon data

Sample	Weight (µg)	U (ppm)	cPb (pg)	Pb* (pg)	Th	206Pb	208Pb	Corrected atomic ratios				207Pb/206Pb	206/238U	207Pb/235U	207/235U Age (Ma)	206/238U Age (Ma)	err	Rho	% disc.	
								(rad.)	%err	(rad.)	%err									(rad.)
20170921 NK-A, Lake Owen complex Lat. 41.18470545, Long. -106.1567458																				
sB	3.79	158	52	1.1	184	0.32	11252	0.092	0.317	-0.17	4.739	-0.21	0.109	-0.11	1774.5	1774.2	1773.7	±2.1	0.84	-0.05
sC	2.69	183	60	1.60	6	0.3	1659	0.086	0.317	-0.13	4.730	-0.23	0.108	-0.18	1773.7	1772.5	1771.1	±3.2	0.64	-0.17
sD	2.69	194	64	1.73	3.3	0.36	3186	0.105	0.318	-0.12	4.743	-0.18	0.108	-0.13	1777.4	1774.9	1771.9	±2.4	0.7	-0.35
sE	1.45	242	82	1.18	3.6	0.44	1987	0.127	0.318	-0.29	4.753	-0.34	0.109	-0.17	1777.6	1776.7	1775.7	±3.1	0.87	-0.12

Notes: sample_s = single grain.

Weight: represents estimated weight after first step of CATIMS zircon dissolution and is only approximate. U and Pb concentrations are based on this weight and are useful for internal comparisons only. Picograms (pg) sample and common Pb from the second dissolution step are measured directly however, and are accurate.

sample Pb: sample Pb (radiogenic + initial) corrected for laboratory blank

cPb: total common Pb. All was assigned to laboratory blank.

Pb*/Pbc: radiogenic Pb to total common Pb (blank + initial)

Corrected atomic ratios: 206Pb/204Pb corrected for mass discrimination and tracer, all others corrected for blank, mass discrimination, tracer and initial Pb, values in

parentheses are 2 sigma errors in percent.

Rho: 206Pb/238U vs 207Pb/235U error correlation coefficient

% disc: percent discordant, - is reversely discordant

Lat. and long. use NAD27

Zircon dissolution and chemistry were adapted from methods developed by Krogh (1973), Parrish et al. (1987) and Mattinson (2005). All zircons were chemically abraded (CATIMS). Final dissolutions were spiked with a mixed 205Pb/233U/235U tracer (ET535). Pb and UO2 from zircons were loaded onto single rhenium filaments with silica gel without any ion exchange cleanup; isotopic compositions were measured in single Daly-photomultiplier mode on a Micromass Sector 54 thermal ionization mass spectrometer at the University of Wyoming. Mass discrimination for Pb was 0.245±0.10 ‰/amu for Daly analyses based on replicate analyses of NIST SRM 981. U fractionation was determined internally during each run. Measured procedural blanks ranged from 2 to 0.38 pg Pb during the course of the study. U blanks were consistently less than 0.1 pg. Isotopic composition of the Pb blank was measured as 18.649±0.403, 15.540±0.29, and 37.804±0.4 for 206/204, 207/204 and 208/204, respectively. Concordia coordinates, intercepts, uncertainties and Concordia Ages were calculated using PbMacDAT and ISOPLLOT programs (based on Ludwig 1988, 1991, 1998); 206Pb/238U and 207Pb/206Pb ratios and dates corrected for Th disequilibrium assuming Th/U magma of 2.2 following Schärer (1984). The decay constants used by PbMacDAT are those recommended by the I.U.G.S. Subcommittee on Geochronology (Steiger and Jäger, 1977): 0.155125 x 10⁻⁹/yr for 238U, 0.98485 x 10⁻⁹/yr for 235U and present-day 238U/235U = 137.88.

Report submitted to the Wyoming State Geological Survey on attempted CATIMS U-Pb zircon and IDTIMS epidote dating of samples from the Albany Quadrangle.

April 12, 2018. Kevin R. Chamberlain, Research Professor, Dept. of Geology and Geophysics, University of Wyoming

Summary

U-Pb dates were attempted from two samples of andesite dikes and three samples of epidote veins in support of the State map of the Albany quadrangle. The zircons recovered from the andesite dikes were so metamict that no reliable date could be determined.

The epidote samples were directly tied to mineralization and regional alteration and their ages would have constrained those processes. Epidote dates have been very useful from several regional studies, particularly Strickland (2004) and Cubrich (2017) however, the epidote from the Albany samples had such low U concentrations and so little spread in Pb/U that no useful geochronologic information was obtained.

Methods

Zircon grains were separated by standard crushing and mineral separation methods. Selected zircons were annealed at 850 °C for 50 hours, then dissolved in two steps in a chemical abrasion, thermal ionization mass spectrometric U-Pb dating method (CATIMS) modified from Mattinson (2005). The first dissolution step was in hydrofluoric acid (HF) and nitric acid (HNO₃) at 180 °C for 12 hours. This removed the most metamict zircon domains in the annealed crystals. Individual grains were then spiked with a mixed ²⁰⁵Pb-²³³U-²³⁵U tracer (ET535), completely dissolved in HF and HNO₃ at 240 °C for 30 hours, and then converted to chlorides. The dissolutions were loaded onto rhenium filaments with phosphoric acid and silica gel without any further chemical processing. Pb and UO₂ isotopic compositions were determined in single Dalyphotomultiplier mode on a Micromass Sector 54 mass spectrometer. Data were reduced and ages calculated using PbMacDat and ISOPLOT/EX after Ludwig (1988, 1991, 1998).

Epidote was separated by chiseling vein occurrences or coarsely crushing samples to liberate pure epidote crystals. Individual crystals were selected for dissolution under a binocular scope. Individual grains or small multi-grain picks were dissolved in HF and HNO₃ at 240 °C for 30 hours, and then converted to chlorides. Aliquots of the solutions were spiked with a mixed ²⁰⁸Pb/²³⁵U spike. Pb and U were purified from both spiked and unspiked aliquots using HBr-HCl ion exchange column chemistry with HNO₃-HCl clean up columns for the U. Pb was run in static multi-collector mode, or single Daly mode to determine the Pb isotopic compositions, using a Micromass S54 thermal ionization mass spectrometer. U was run as a metal, loaded with graphite.

Results

Andesite dike 20170912NK-G (Lat. 41.174711, Long. -106.234870): Two samples of the andesite dike were processed for dating. Both samples had abundant titanite, which is likely metamorphic based on titanite dates from nearby samples (Strickland 2004; Cubrich 2017). This sample also had a few metamict zircons (Figure 1), which were targeted for dating to try to establish the magmatic age of the dike. Only one of the selected zircons survived the first step of partial dissolution in three attempts. The data from that one point is extremely reversely discordant (-121%, Figure 2) due to uranium loss during the first partial dissolution. The ²⁰⁷Pb/²⁰⁶Pb date of this grain, 1624±50 Ma (Table 1) is the best estimate of the magmatic age of the dike, but as this is only a single analysis, I don't place much confidence in the date. The CATIMS process removed significant amount of common Pb from the zircon as indicated in a Pb-Pb plot (Figure 3). To try to support this date, 3 separate zircons were dissolved whole, without any chemical abrasion. Those data are extremely normally discordant (75 to 90%, Figure 2) and plot in a non-linear array. The discordance is likely due to natural Pb loss in such metamict grains. Pb-Pb data from these total dissolution zircons are also non-linear (Figure 3) and do not support the CATIMS data.

Epidote samples Five samples were collected for epidote dating, grains from three of these were dissolved and analysed for U-Pb dating:

2017824NK-F: Cuprite mine *Lat. 41.1983853, Long. -106.2411104*

2017825NK-A: Collapsed adit and shaft on Florence trend *Lat. 41.16538835, Long. 106.2486765*

2017825NK-E: *Prospect pit on Florence trend Lat. 41.16200122, Long. -106.2465152* Individual grains with distinctive differences in color were selected to test whether there was sufficient variation in U/Pb and spread in Pb ratios to generate isochrons. The data from all three samples are plotted in Figure 4, none of the data from an individual sample have enough spread to generate reliable dates, the uncertainties are 500 to 1300 Ma. If the two Florence trend samples, 25NK-A&E, formed at the same time from the same fluids, then their data could be combined. The isochron date from combining these two samples has a slope of about 1564 Ma, which is a reasonable date for epidote in the southern Medicine Bow Mountains (Strickland 2004; Cubrich 2017), but the uncertainty is ± 190 Ma, so the epidote event is very poorly constrained. Epidote from the other two samples may have higher U concentrations and more variation in Pb/Pb ratios.

References (including Tables 1):

Cubrich, B.T., 2017, Paleoproterozoic history of the Rocky Mountains: using multiple geochronologic methods to unravel the Proterozoic structural history of polyphase deformation in highly deformed rocks. [*MS thesis*]: Laramie, University of Wyoming.

Krogh, T.E., 1973, A low-contamination method for hydrothermal decomposition of zircon and extraction of U and Pb for isotopic age determinations: *Geochimica et Cosmochimica Acta*, v. 37, p. 485–494.

Krogh, T.E., Corfu, F., Davis, D.W., Dunning, G.R., Heaman, L.M., Kamo,

S.L., Machado, N., Greenough, J.D., and Nakamura, E. 1987. Precise U-Pb isotopic ages of diabase dykes and mafic to ultramafic rocks using trace amounts of baddeleyite and zircon. In *Mafic dyke swarms*. Edited by H.C. Halls and W.F.

Fahrig, Geological Association of Canada, Special paper 34, pg 147-152.

Ludwig, K.R., 1988, PBDAT for MS-DOS, a computer program for IBM-PC compatibles for processing raw Pb-U-Th isotope data, version 1.24: U.S. Geological Survey, Open-File Report 88-542, 32 pp.

Ludwig, K.R., 1991, ISOPLOT for MS-DOS, a plotting and regression program for radiogenic-isotope data, for IBM-PC compatible computers, version 2.75: U.S.

Geological Survey, Open-File Report 91-445, 45 pp.

Ludwig, K. R., 1998, On the treatment of concordant uranium-lead ages. *Geochimica et Cosmochimica Acta*, 62(4), 665-676.

Mattinson, J.M., 2005, Zircon U-Pb chemical abrasion (“CA-TIMS”) method: combined annealing and multi-step partial dissolution analysis for improved precision and accuracy of zircon ages: *Chemical Geology*, v. 220, p. 47-66.

Parrish, R.R., Roddick, J.C., Loveridge, W.D., and Sullivan, R.D., 1987, Uranium-lead analytical techniques at the geochronology laboratory, Geological Survey of Canada, *in Radiogenic age and isotopic studies*, Report 1: Geological Survey of Canada Paper 87-2, p. 3–7.

Stacey, J.S. and Kramers, J.D., 1975, Approximation of terrestrial lead isotope evolution by a two-stage model: *Earth and Planetary Science Letters*, v. 26, p. 207–221.

Steiger, R.H. and Jäger, E., 1977, Subcommittee on geochronology: convention on the use of decay constants in geo- and cosmochronology: *Earth and Planetary Science Letters*, v. 36, p. 359–362.

Strickland, D., 2004. Structural and Geochronologic Evidence for the Ca. 1.6 Ga Reactivation of the Cheyenne Belt. *Southeastern Wyoming [MS thesis]: Laramie, University of Wyoming.*



Figure 1. Examples of large, metamict zircons from the andesite dike sample 20170912 NK-G. These were the only zircons recovered from either dike sample.

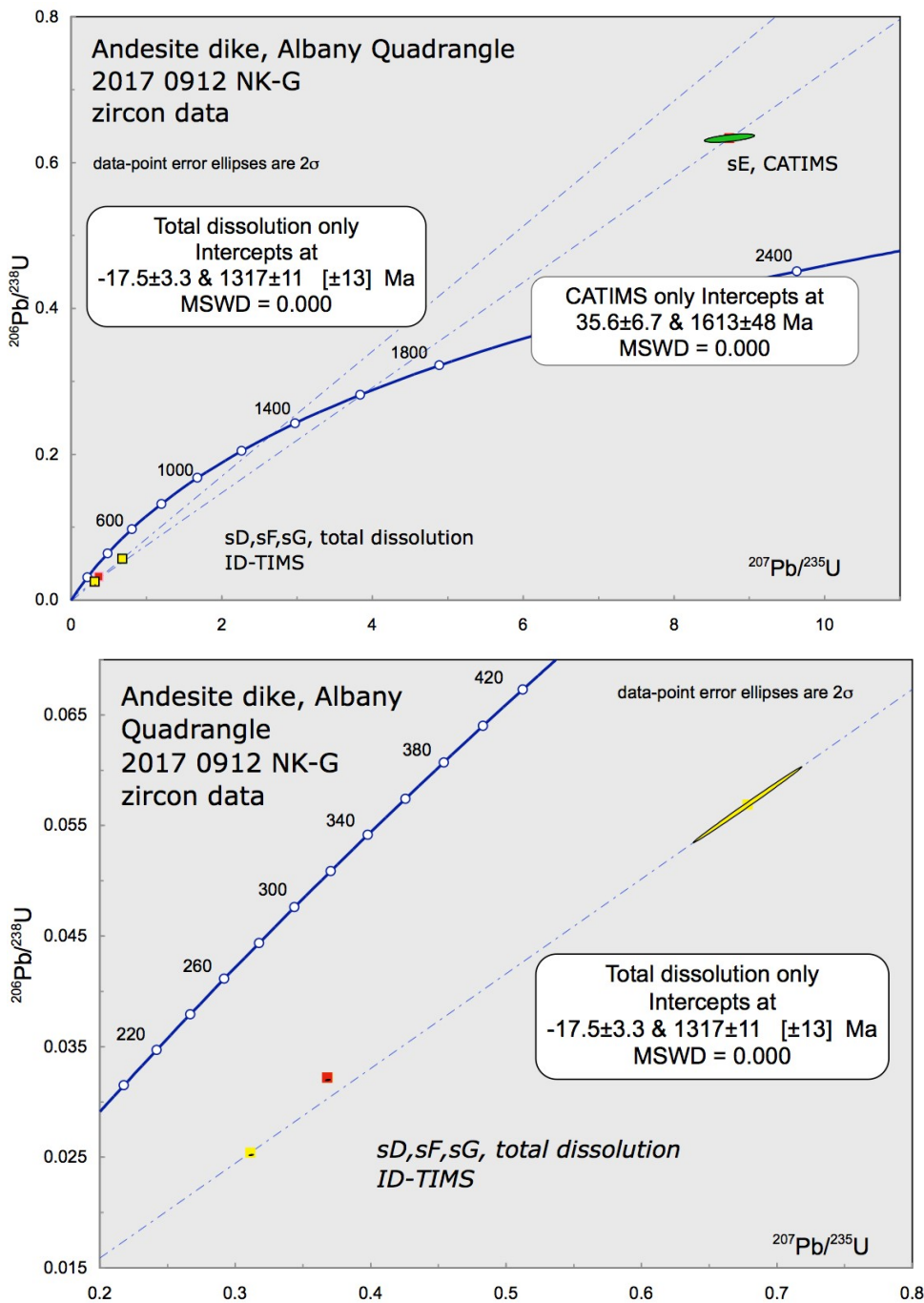


Figure 2. Concordia plot of 4 single zircon analyses from 20170921NK-G, andesite dike in the Albany quadrangle, SE Wyoming. All data in upper plot, showing reverse discordance in CATIMS analysis, probably due to laboratory-induced uranium loss, and extreme normal discordance in the total dissolution analyses, probably due to natural Pb loss in such metamict zircons. Lower plot, close up of 3 total dissolution data points showing non-linearity.

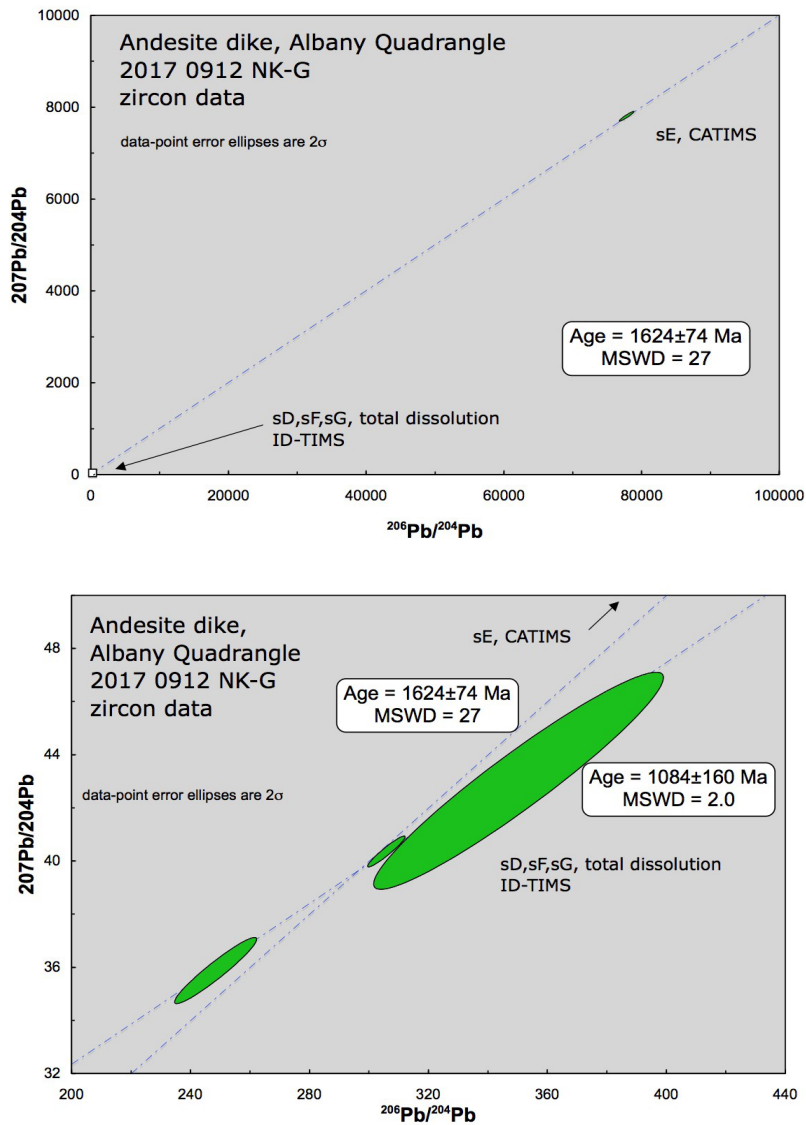


Figure 3. Pb-Pb plots of zircon data from andesite dike sample 20170912 NK-G from the Albany quadrangle. Upper plot demonstrates that the CATIMS method removed much of the common Pb from the analyzed zircon (sE). Lower plot is closed up of the total dissolution data, showing non-linearity in the data. No date interpretation is supported by these data.

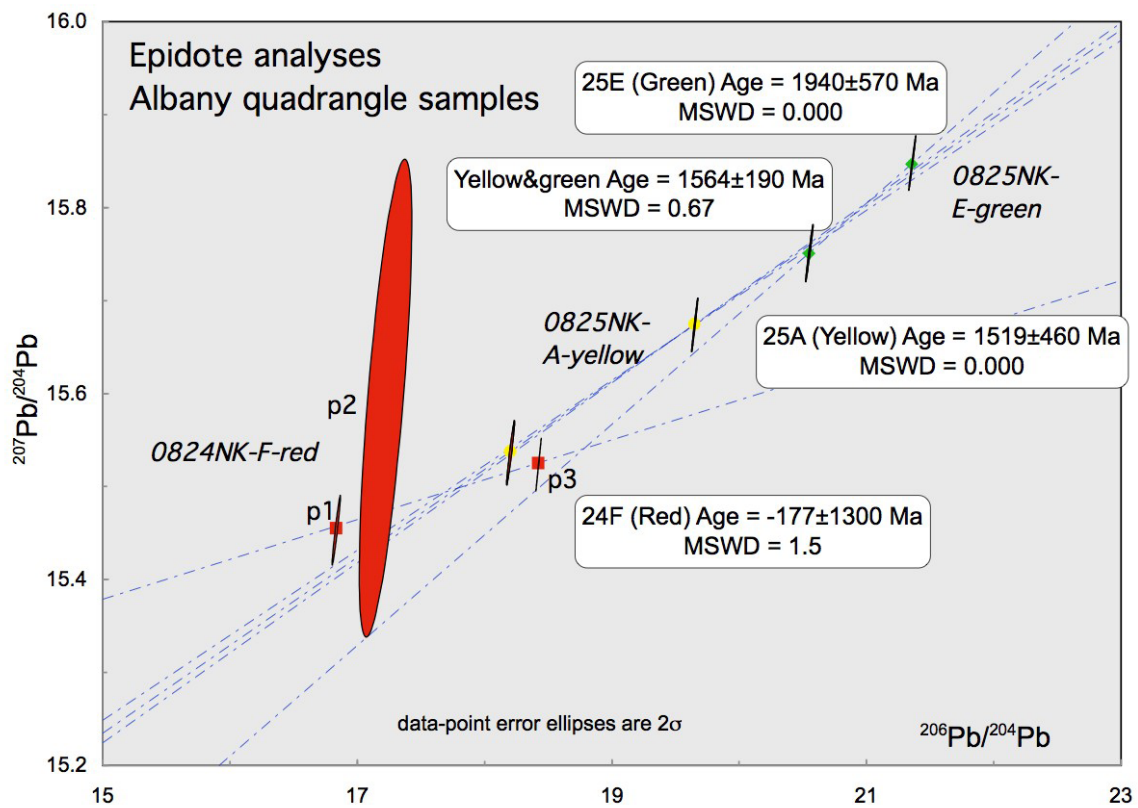
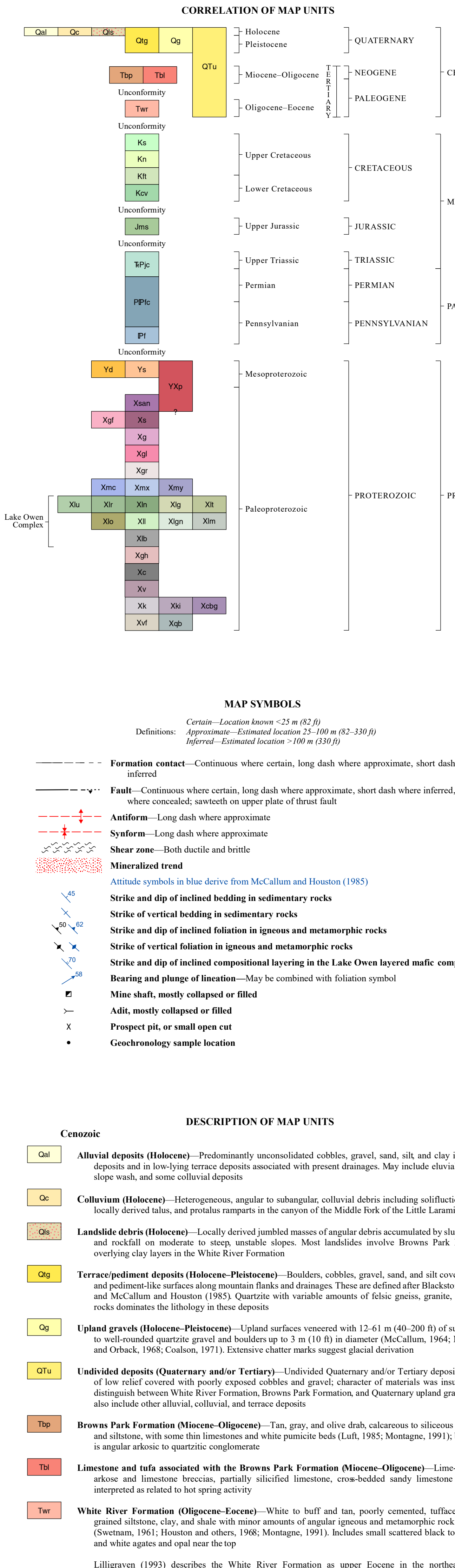
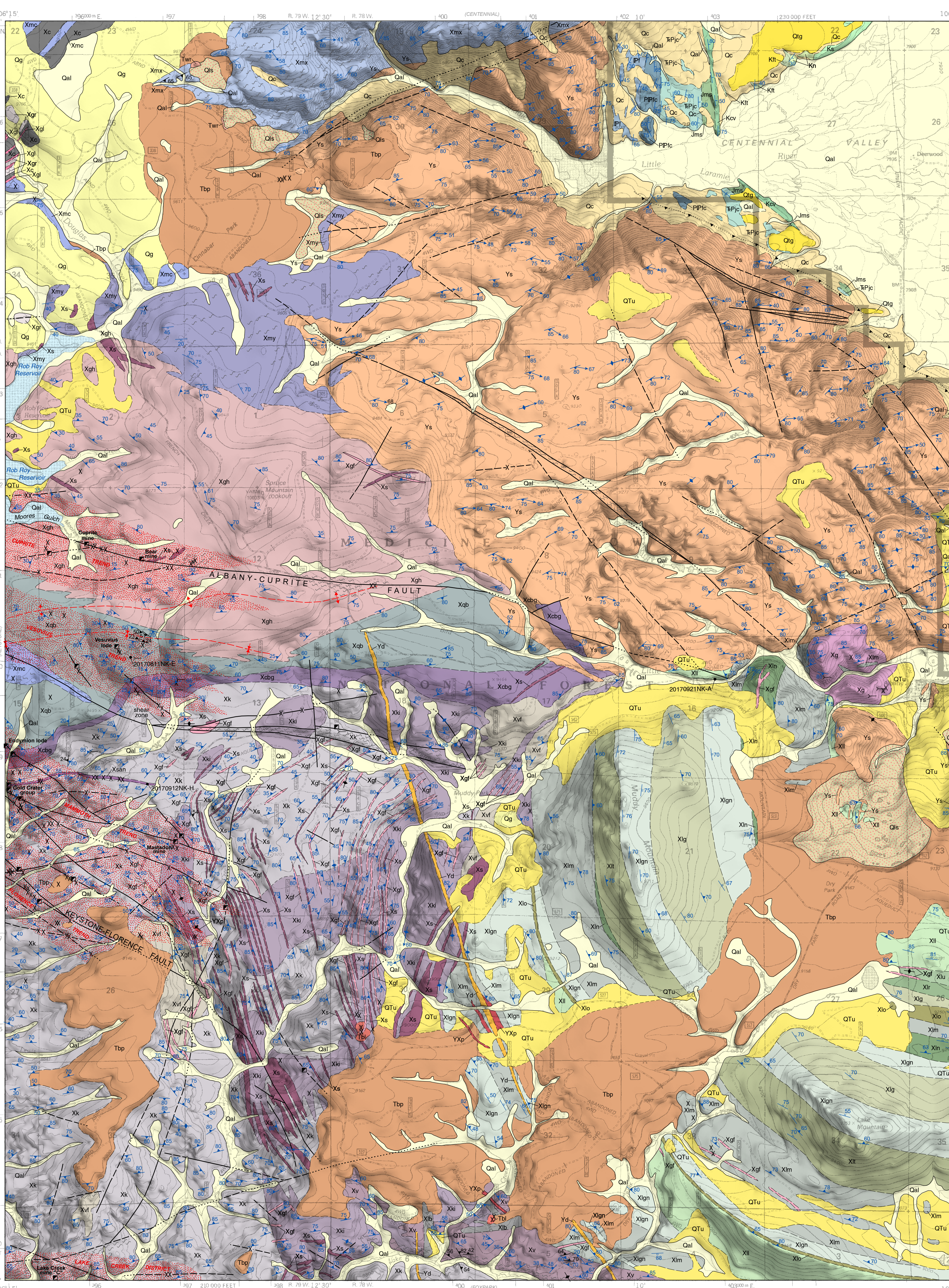


Figure 4. Pb-Pb plot of all epidote from 3 different samples. None of the samples displayed enough spread in Pb values to generate a precise date. Even combining data from two samples, 25E and 25A (which would require assuming they grew at the same time from the same fluids), still has high enough uncertainty that the epidote growths could have occurred over a 400 Ma period in the Paleoproterozoic.



Interpreting the past, providing for the future



EXPLANATION

Precambrian

Yd Dike (Mesoproterozoic)—Undeformed and unmetamorphosed, fine- to medium-grained, pink to pink-orange to gray, magnetite-rich, porphyritic quartz latite, quartz-rich with small amounts of plagioclase, sphene, epidote, and biotite (McCallum and Houston, 1985); may be of more than one age (Houston and others, 1963); no fabric observed in outcrops.

Ys Sherman Granite (Mesoproterozoic)—Pink, medium- to coarse-grained, faintly foliated granite dated at 1,433 ± 1.5 Ma by Frost and others (1999). A younger coarse-grained porphyritic phase also present (McCallum and Houston, 1985). Contacts with older rocks typically sharp. Plagioclase, microcline, and quartz tend to be equigranular, but biotite is highly variable in size. Local hybridization of both granite and country rock at contacts with mafic bodies. Struck-slip and flattened textures of earlier rock types common but not abundant. Locally deep red and enriched in epidote and quartz where sheared or brecciated.

Yxo Pegmatite (Mesoproterozoic-Paleoproterozoic?)—Pink to white pegmatites consisting primarily of quartz, microcline, and muscovite, locally accompanied by abundant small grains; crystal sizes 2 mm to 30 cm (0.08 to 12 in). Sharp, chilled margins, alternating layers of fine and coarse crystals on the outer edges, found throughout the quadrangle, but most too small to map. Larger occurrences in the south central part of the quadrangle, either cutting or near to the Lake Owen layered mafic complex. Generally conformable to the foliation of the rocks in which they intrude (McCallum and Houston, 1985). May be of more than one age (Houston and others, 1968).

Yxn Andesite dike (Paleoproterozoic)—Several small red-brown dikes and one east-trending dike large enough to map in west-central part of quadrangle. Intruded along fault zones, and locally sheared and chloritized (McCallum and Houston, 1985). Fine-grained, biotite-rich, pigmentite andesite grades into hornblende-rich varieties. Primary minerals are quartz, biotite, epidote, and plagioclase. Numerous prospects along these dikes.

Xs Mafic intrusive rocks (Paleoproterozoic)—Dikes are most abundant where cutting eastern portions of Keystone Quartz Diorite west of the Lake Owen complex. Dark-gray-green to black dikes generally less than 5 m (16 ft) thick, fine- to medium-grained, with minor coarse-grained parts. Varies from basaltic to gabbro, metabasalt, and diabase. Chilled margins, moderately altered to completely amphibolized (McCallum and Houston, 1985). Amphibole rich to biotite rich, with variable plagioclase, quartz, and opaque minerals. Hornblende may be actinolitic and chloritized, with accessory magnetite, ilmenite, and epidote, and some relic clinopyroxene.

Xgf Small felsic intrusives (Paleoproterozoic)—Small felsic intrusives contain quartz, microcline, albite, and biotite, with occasional hornblende and magnetite hematite. Generally fine- to medium-grained with near-equal fabric. Minor coarse-grain occurrences, most abundant in southern and eastern parts of quadrangle. Irregular sills 1.5 m (10–50 ft) thick, 1 km (0.6 mi) long or longer. Typically accentuate structural trends of intruded rock, with both concordant and discordant contact relationships. Interpreted as both sills to post-shear intrusions (McCallum and Orback, 1968; Ramirez, 1971).

Xg Older granite (Paleoproterozoic)—Distinct red to orange, coarse-grained, foliated granite northwest of the Lake Owen complex. About 60 percent plagioclase/potassium feldspar with quartz, biotite, and magnetite, and uncommon xenoliths of Lake Owen mafic complex. Houston and others (2003) equate it to quartz monzonite and similar rocks in other parts of the Medicine Bow Mountains.

Xgl Luxullianite (Paleoproterozoic)—Generally concordant, locally zoned, medium-grained, pink to pinkish-white, hornblende-rich (up to 30 percent), lenticular to rock- and dike-like bodies intruding into mylonitic gneiss and amphibolized metagabbros near the Rambler splay of the Mullen Creek-Nash Fork shear zone (Houston and McCallum, 1961; McCallum, 1964). Considered a late phase of the Rambler granite (McCallum and Orback, 1968; Coakson, 1971). Includes plagioclase (albite), quartz, microcline, hornblende, muscovite, sericite, and garnet, with schorl crystals up to several inches long in pegmatitic phases. Rb-Sr whole rock isochron of 1,699 ± 40 Ma (Hills and Houston, 1979).

Xgr Rambler granite (Paleoproterozoic)—Medium- to coarse-grained, pink to red, microcline-rich granite, cataclastically foliated with abundant epidote along shear planes. Consists of quartz, potash feldspar, sodic plagioclase, biotite, and chlorite with minor amounts of epidote, hornblende, muscovite, magnetite, and allanite (McCallum and Orback, 1968; Coakson, 1971). Exposed only in the northwest corner of the quadrangle. Both conformable and cross-cutting relationships with surrounding rocks. Dated 1,770.8 ± 3.4 Ma (Premo and Loucks, 2000).

Xnc Cataclastic textured rocks (Paleoproterozoic)—Fine-grained rocks within shear zones, with variable weathering textures from almost sandy or silty to phyllite and mylonite. Commonly silicified and jarvisized. Most extensive in the northwestern part of the quadrangle, with similar rocks in the west-central part of quadrangle.

Xnx Mixed units within the Rambler splay of the Mullen Creek-Nash Fork shear zone (Paleoproterozoic)—Various rock type sills and sheared to mylonitic rocks associated with the fault zone and post-shear exposures within the Rambler splay of the Mullen Creek-Nash Fork shear zone. Includes calc-silicate gneiss, marble, amphibole gneiss, quartzofeldspathic gneiss, mylonitic gneiss, and others (McCallum and Houston, 1985).

Xny Mylonitic gneiss (Paleoproterozoic)—Distinct pink to buff or gray, locally black, very fine to medium-grained gneiss with moderate to well-developed cataclastic to mylonitic fabric and pronounced flow structure. Predominantly felsic but includes lenses, stringers, and layers of mafic rock. Mineralogically variable, but typically quartz-rich with equal amounts of potassium feldspar and plagioclase accompanied by significant biotite, which is locally chloritized. Accessory minerals include magnetite, ilmenite, epidote, titanopyroxene, and muscovite (McCallum and Houston, 1985). Occurs in the northwestern part of the quadrangle.

Lake Owen layered mafic complex (Paleoproterozoic)—Large, roughly circular, intermittently layered mafic intrusion of approximately 54 sq km (21 sq mi) consisting of gabbro, olivine gabbro, norite, olivine norite, and troctolite, all locally gradational with one another. Cuts adjacent gneiss units, and is cut by Keystone Quartz Diorite on the west and by Sherman Granite on the north. Pegmatite gabbro-norite rock within the layered unit yielded a 2018 U-Pb zircon age of 1,775.1 ± 3.0 Ma (sample number 20170921NK-A).

Xlu Olivine magnetite gabbro-norite—Dark gray to black with highly variable magnetite content ranging from 3–28 percent and averaging about 8 percent (Houston and others, 2003).

Xli Magnetite gabbro-norite—Dark gray to purple, with a higher proportion of mafic minerals than gabbro-norite, including 7–15 percent cumulate magnetite (Houston and others, 2003). Prominent magnetite gabbro-norite within unit is interlayered with gabbro-norite.

Xln Norite—Dominantly gray, varying to orange, medium- to coarse-grained, unlayered to subtle layers that result from alteration of plagioclase- and pyroxene-rich layers, and the preferred orientations of plagioclase. Pyroxenes tend to be green and dominantly lengthened along the *ax*-axis; orange weathering attributed to hematite plates in plagioclase (Houston and others, 2003).

Xlg Gabbro—Dark gray to greenish black, to orange weathering, medium to coarse grained. Plagioclase laths are preferentially oriented. Lower magnetite content than other members of the complex (McCallum and Houston, 1985).

Xli Troctolite—Light-gray to gray unit dominated by troctolite. Well-developed preferred orientation of plagioclase laths. Oxidation of large olivine crystals results in localized brownish-red spotted texture. Interlayers of anorthite and clinopyroxene are common (McCallum and Houston, 1985).

Xlo Olivine gabbro—Dark gray to reddish-brown, fine-grained gabbro forms relatively resistant ridges. Coarser grain size near top of the unit (Houston and others, 2003). Strong preferred orientation in plagioclase laths. Olivine in weathered samples alters to dark brown and locally leaves voids where partially to completely destroyed (McCallum and Houston, 1985). Unoxidized olivine not always obvious in hand samples.

Xli Layered unit—Alternating light and dark layers of olivine gabbro-norite, troctolite, and norite, varying in thicknesses from a few cm to a few meters (10 to 100 ft). Magnetite content, includes some cyclical layers of olivine gabbro-norite alternating with layers of norite. Cyclical layers and lenses exhibit gradational changes in crystal size from fine to megacrystic over short distances and are locally accompanied by sulfides. Pegmatite sample provided a radiometric date for the Lake Owen complex.

Xlgn Gabbro-norite—Dark brown, dark gray, and black mineral-grained layers with dark pyroxene between overlain by light plagioclase-rich tops. Layers separated by thick unlaminated gabbro-norite with preferred mineral orientations. Some magnetite gabbro layers, particularly near the top (Houston and others, 2003). Plagioclase varies from smoky to deep, dark gray, with both ortho- and clinopyroxene in variable ratios, accompanied by hornblende and sphene.

Xlm Magnetite gabbro—Dark brown to purplish-gray and black, magnetite-rich (generally 70–90 percent magnetite); equigranular with blocky, stubby, fine- to medium-grained crystals, disseminated magnetite is dominant, distinct massive magnetite layers and lenses 30 cm (12 in) thick also occur. Much of magnetite appears to be cumulate and occurs interstitially, in microvoids, and/or replacing silicate minerals (McCallum and Houston, 1985).

Xlb Border phase—Dark-gray to black and porphyritic basalt, locally brecciated and filled with gabbro, exhibiting effects of contact metamorphism (Houston and others, 2003) and mixing with adjacent rock types. Appearance varies from breccia to glass to solid basalt. Epidote-rich with common felsic veining.

Xgp Horse Creek foliated granodiorite (Paleoproterozoic)—Pink to buff or light-gray sill-like to interfingering (mostly perthitic) and biotite. Accessory muscovite, epidote, and minor hornblende, potassium feldspar, titanite-sphene, and allanite (McCallum and Orback, 1968). Predominantly fine- to medium-grained with lesser coarse-grained phases, unfoliated to conspicuously foliated. Zones of moderate to severe cataclasis (McCallum and Orback, 1968). U-Pb zircon age of 1,777 ± 4 Ma (Premo and Van Schmus, 1989).

Xc Mullen Creek layered mafic complex (Paleoproterozoic)—Large, irregularly shaped body of fine- to coarse-grained mafic gneiss and metagabbros, locally layered rocks south of the Cheyenne belt. Remembers Lake Owen complex (Loucks and Glascock, 1989), but much more metamorphosed and deformed. Includes gabbro, olivine gabbro, norite, leucogabbro, anorthositic diorite, basalt/diabase, and pyroxenite, commonly sheared, and partially to completely amphibolized. Exposed as prominent, massive, rounded to spherical blocks bounded by widely spaced joints. A U-Pb zircon age of 1,777.6 ± 2.1 Ma (Loucks, Premo, and Snyder, 1988).

Xv Metavolcanic and metasedimentary gneiss and schist (Paleoproterozoic)—Highly variable, interlayered, amphibole-grained metavolcanic and metasedimentary gneiss and schist (Houston and others, 2003) near the south-central edge of the quadrangle. Fine-grained, slightly to highly foliated, light to dark gray to deep-orange-pink and light-pink gneiss composed principally of potassium feldspar, quartz, plagioclase, hornblende, biotite, and accessory epidote. Banded where composition cycles between mafic and felsic, with irregular large mafic to felsic variations. Common shearing is both brittle and ductile. Rhyolite in the adjacent Fort Cobb quadrangle to the south was dated at 1,778.4 ± 1.7 Ma (Carnes and others, in press).

Xk Keystone Quartz Diorite (Paleoproterozoic)—Gray to whitish-gray to pink, medium- to coarse-grained, locally porphyritic, weakly to strongly foliated quartz diorite. Dominated by plagioclase with roughly equal amounts of quartz, and up to 30 percent hornblende. Accessory biotite, epidote, chlorite, microcline, and titanite-sphene (Curry, 1965; Houston and others, 1968). Contacts with adjacent pre-existing metamorphic rocks are commonly gradational. Exposed as prominent, massive, rounded to spherical blocks bounded by widely spaced joints. A U-Pb zircon age of 1,784.7 ± 1.9 Ma (Campbell and Shelton, 2017).

Xki Keystone Quartz Diorite transition zone (Paleoproterozoic)—Gradational contact transition zone between Keystone Quartz Diorite and adjacent pre-existing rocks. Varies from a few cm to greater than 183 m (600 ft) wide (Curry, 1965; Houston and others, 2003; Sutherland and Hansel, 2005). Gneiss zone within the quartz diorite decreases and foliation is stronger when nearing contact. Quartz diorite partially replaces, or is injected into the folia of older rocks. Xenoliths, sills, and lenticular bodies exhibit varying degrees of hybridization and locally comprise more than 30 percent of exposures (McCallum and Houston, 1985).

Xkb Contorted boundary gneiss (Paleoproterozoic)—Distinct transition unit between Keystone Quartz Diorite and biotite gneiss extending eastward across the center of the quadrangle. Very fine crystals and gneiss exhibiting dramatic small-scale folds and crenulations. Coarse-grained felsic igneous complex.

Xkf Quartzofeldspathic gneiss (Paleoproterozoic)—Light-pink, weathering to very dark pink gneiss with variable composition, dominated by plagioclase, quartz, biotite, and epidote, with trace hematite/magnetite, and mafic content of 10–15 percent. Weak gneiss fabric, locally sheared, and exposed in southwest part of the quadrangle.

Xkb Quartz-biotite gneiss (Paleoproterozoic)—Dense, gray to black to pinkish-gray; brown where weathered, dominated by biotite and quartz, with variable amounts of plagioclase, potassium feldspar, opaque minerals, epidote, muscovite, chlorite, amphibole and titanite-sphene (McCallum and Houston, 1985). Mapped as quartz-biotite schist in the Keystone quadrangle to the west where it is 732 m (2,400 ft) thick (Curry, 1965; Sutherland and Hansel, 2005). Moderately to well-developed foliation defined by alignment of biotite, lenses of accessory minerals (primarily epidote), or planar zones of differential cataclasis. Abundant passive folds, grading laterally into more pinkish-white, medium- to coarse-grained biotite-plagioclase gneiss mapped separately by McCallum and Houston (1985) where plagioclase increases to as much as 65 percent. Local minor quartzite suggests a partial metasedimentary component.

Mesozoic

Xkc Steele Shale (Upper Cretaceous)—Predominantly dark-gray marine shale, interbedded in the upper part with thin beds of fine-grained, buff to orange-weathering, brown sandstone and siltstone. Thickness estimated at 823 (±2,700 ft) by Houston and Orback (1976).

Xkn Niobrara Formation (Upper Cretaceous)—Highly fossiliferous, predominantly gray, calcareous shale, interbedded with cream to yellow and orange-weathering siltstone (Blackstone, 1970; Houston and Orback, 1976). Up to 152 m (500 ft) thick.

Xkr Frontier Formation and Mowry Shale (Upper Cretaceous), and Thermopsis Shale (Lower Cretaceous), undivided—Estimated thickness of 210–279 m (690–915 ft) for combined units.

Frontier Formation—Gray to black shale, interbedded biotite, and the Wall Creek Sandstone near the top; siliceous septarian concretions abundant near the base. Ranges from 140–183 m (460–600 ft) (Houston and Orback, 1976).

Mowry Shale—Dark-gray to black, siliceous, silver-gray-weathering shale with numerous thin bentonitic beds near the top. Ranges from 37–50 m (120–165 ft) thick (Blackstone, 1970; Houston and Orback, 1976).

Thermopsis Shale—Black to dark-brown marine shale with brown to olive-green, fine-grained sandstone layers that host bedding planes covered with tubular structures interpreted as worm burrows. Ranges from 34–46 m (112–150 ft) thick (Blackstone, 1970; Houston and Orback, 1976).

Chocoma Formation (Lower Cretaceous)—Consists of an upper reddish-brown to yellow, iron-stained, thin-bedded sandstone, a middle pink shale and gray to pink siltstone, and a basal, locally conglomeratic, cross-bedded, white sandstone that locally hosts pebble-sized clasts of quartz and chert. Approximately 52 m (170 ft) thick (Blackstone, 1970; Houston and Orback, 1976). Some sandstones silica-cemented to form orthoquartzites.

Morrison and Sundance formations, undivided (Upper Jurassic)

Morrison Formation—White sandstone beds near the top underlain by varicolored bluish-gray, purple, deep-red, and gray shale with lenticular beds of white, cross-bedded, fine-grained sandstone and gray nodular limestone. Approximately 91 m (300 ft) thick (Blackstone, 1970; Houston and Orback, 1976).

Sundance Formation—White to pale-yellow, cross-bedded and ripple-marked, calcareous, glauconitic sandstone and siltstone, with gray and green shale in the lower part. Abundant *Pachytrephites densus* (thick-walled bellerophonid form) found in the upper part. Approximately 15 m (50 ft) thick (Blackstone, 1970; Houston and Orback, 1976).

Laft, S.J., 1985. Generalized geologic map showing distribution and basal configuration of the Browns Park Formation and Bishop Conglomerate in northwestern Colorado, northeastern Utah, and southern Wyoming. U.S. Geological Survey Miscellaneous Field Studies Map MF-182-1, scale 1:250,000.

McCallum, M.E., 1964. Petrology and structure of the Precambrian and post-Mississippian rocks of the east-central Medicine Bow Mountains, Albany and Carbon counties, Wyoming. Laramie, University of Wyoming, Ph.D. dissertation, 164 p.

McCallum, M.E., and Houston, R.S., 1985. Geologic map of the Albany quadrangle, Albany County, Wyoming. (unpublished mineral files): Geological Survey of Wyoming [Wyoming State Geological Survey]. 16 p., 1 pl., scale 1:24,000.

McCallum, M.E., and Orback, C.J., 1968. The New Rambler copper-gold-platinum district, Albany and Carbon counties, Wyoming. Geological Survey of Wyoming [Wyoming State Geological Survey] Preliminary Report 8, 12 p., 1 pl., scale 1:24,000.

Montagne, John, 1991. Cenozoic history of the Saratoga Valley area, Wyoming and Colorado. Contributions to Geology, v. 29, no. 1, p. 13–70, 1 pl., scale approx. 1:163,510.

Premo, W.R., and Loucks, R.R., 2000. Age and Pb-Sr-Nd isotopic systematics of plutonic rocks from the Green Mountain magmatic arc, southeastern Wyoming—Isotopic characterization of a Paleoproterozoic island arc system. Rocky Mountain Geology, v. 35, no. 1, p. 51–70.

Premo, W.R., and Van Schmus, W.R., 1989. Zircon geochronology of Precambrian rocks in southeast Wyoming and northern Colorado, in Grantling, J.A., and Tewksbury, B.J., eds., Proterozoic geology of the southern Rocky Mountains. Geological Society of America Special Paper 235, p. 13–32.

Ramirez, Octavio, 1971. Petrology and structure of the Precambrian metagneiss sequence in the Savage Run Creek area, Carbon County, Wyoming. Fort Collins, Colorado State University, M.S. thesis, 117 p., 1 pl., scale 1:16,000.

Sutherland, W.M., and Hansel, W.D., 2005. Preliminary geologic map of the Keystone quadrangle, Albany and Carbon counties, Wyoming. Wyoming State Geological Survey Open File Report 05-6, 22 p., 1 pl., scale 1:24,000.

Swetnam, M.N., 1961. Geology of the Pelton Creek area, Albany and Carbon counties, Wyoming. Laramie, University of Wyoming, M.S. thesis, 78 p., 1 pl., scale 1:15,500.

Ver Ploeg, A.J., Larsen, M.C., and Taboga, K.G., 2016. Characterization of evaporitic salt features in the southern Laramie Basin, Wyoming. Wyoming State Geological Survey Report of Investigations 70, 34 p.

Mesozoic and Paleozoic

Xpt Jelm Formation (Upper Triassic) and Chugwater Formation (Triassic-Permian), undivided

Jelm Formation—Orange and red siltstone and sandstone overlying a distinctive calcipellitic conglomerate, which may include fragments of vertebrate bones and crosscut teeth. Ranges from 40–76 m (130–250 ft) thick (Houston and others, 1985; Love and others, 1993).

Chugwater Formation—Thinly bedded calcareous red shales, siltstones, and local thin sandstones with some thin beds of limestone and gypsum (anhydrite) approximately 168–229 m (550–750 ft) thick (Houston and others, 1968; Blackstone, 1970; Houston and Orback, 1976; Love and others, 1993; Ver Ploeg and others, 2016).

Paleozoic

Xpp Forelle Limestone, Satanka Shale (Permian), and Casper Formation (Permian-Pennsylvanian), undivided

Forelle Limestone—Resistant, lavender to gray and white, crinellated limestone at the top of the Satanka Shale with thin red to gray shale or siltstone in the middle. Ranges from 3–6 m (10–20 ft) thick (Houston and others, 1968; Blackstone, 1970; Houston and Orback, 1976).

Satanka Shale—Orange to red siltstones and shales containing thin lenticular beds of gypsum, limestone, and ferruginous sandstone. Ranges from 37–67 m (120–220 ft) thick (Houston and others, 1968; Blackstone, 1970; Houston and Orback, 1976).

Casper Formation—Upper part yellowish to pink, buff, and white, fine- to medium-grained calcareous sandstone with well-developed festoon cross-bedding and abundant orange chert grains; middle part red and gray, hard siltstone and shale with some thin gray limestone beds; lower part white and red, cross-bedded sandstone; conglomerates at the base. Approximately 63 m (207 ft) thick (Houston and others, 1968; Blackstone, 1970; Houston and Orback, 1976).

Xpi Fountain Formation (Pennsylvanian)—Pink to maroon, calcareous, arkosic sandstone with lesser beds of light-purple arkose, gray sandstone, red siltstone, red shale, and white limestone. A few interbedded conglomerates. Beds discontinuous with variable thicknesses, cross-bedded sandstone and conglomerate channel fills common. Ranges from 122 m (400 ft) to more than 152 m (500 ft) thick (Houston and others, 1968; Blackstone, 1970; Houston and Orback, 1976).

PRELIMINARY GEOLOGIC MAP OF THE ALBANY QUADRANGLE, ALBANY COUNTY, WYOMING

by
Wayne M. Sutherland and Natali A. Krahn
2018

REFERENCES

Blackstone, D.L., Jr., 1970. Structural geology of the Rex Lake quadrangle, Laramie Basin, Wyoming. Geological Survey of Wyoming [Wyoming State Geological Survey] Preliminary Report 11, 17 p., 1 pl., scale 1:24,000.

Campbell, E.A., and Shelton, C.R., in press. Preliminary geologic map of the Woods Landing quadrangle, Albany County, Wyoming. Wyoming State Geological Survey Open File Report 2018-3, scale 1:24,000.

Carnes, J.D., Chamley, A.S., and Sams, C.P., in press. Preliminary geologic map of the Foxpark quadrangle, Albany County, Wyoming. Wyoming State Geological Survey Open File Report 2018-5, scale 1:24,000.

Coakson, E.B., 1971. Geology of the New Rambler mine area, Albany County, Wyoming. Laramie, University of Wyoming, M.S. thesis, 51 p., 1 pl., scale 1:12,000.

Curry, D.R., 1965. The Keystone gold-copper prospect area, Albany County, Wyoming. Geological Survey of Wyoming [Wyoming State Geological Survey] Preliminary Report 3, 12 p., 1 pl.

Frost, D.C., Frost, B.R., Chamberlain, K.R., and Edwards, B.R., 1999. Petrogenesis of the 1.43 Ga Sherman batholith, SE Wyoming, USA—A reduced rapakivi-type anorthositic granite. *Journal of Petrology*, v. 40, no. 12, p. 1771–1802.

Hills, F.A., and Houston, R.S., 1979. Early Proterozoic tectonics of the central Rocky Mountains, North America. *Contributions to Geology*, v. 17, no. 2, p. 89–109.

Houston, R.S., and others, 1968. A regional study of rocks of Precambrian age in that part of the Medicine Bow Mountains lying in southeastern Wyoming—With a chapter on the relationship between Precambrian and Laramie structure. Geological Survey of Wyoming [Wyoming State Geological Survey] Memoir 5, v. 1, p. 78–116.

Houston, R.S., Karlstrom, K.E., Hills, F.A., and Smithson, S.B., 1979. The Cheyenne belt—A major Precambrian crustal boundary in the western United States (abs). *Geological Society of America Special Paper* 11, p. 446.

Houston, R.S., and McCallum, M.E., 1961. Mullen Creek-Nash Fork shear zone, Medicine Bow Mountains, southeastern Wyoming (abs). *Geological Society of America Special Paper* 68, p. 91.

Houston, R.S., McCallum, M.E., and Patchen, A.D., 2003. Geologic map of a portion of the Lake Owen and Albany quadrangles, Albany County, Wyoming, showing major lithologic subdivisions of the Lake Owen mafic complex (unpublished mineral files): Wyoming State Geological Survey, scale 1:24,000.

Houston, R.S., and Orback, C.J., 1976. Geologic map of the Lake Owen quadrangle, Albany County, Wyoming. U.S. Geological Survey Geologic Quadrangle Map GQ-1304, scale 1:24,000.

Houston, R.S., and others, 1968. A regional study of rocks of Precambrian age in that part of the Medicine Bow Mountains lying in southeastern Wyoming—With a chapter on the relationship between Precambrian and Laramie structure. Geological Survey of Wyoming [Wyoming State Geological Survey] Memoir 5, v. 1, p. 78–116.

Lilligren, J.A., 1993. Correlation of Paleozoic strata across Wyoming—A users' guide. In Snook, A.W., Stredlmann, J.R., and Roberts, S.B., eds., *Geology of Wyoming: Geological Survey of Wyoming [Wyoming State Geological Survey] Memoir 5*, v. 1, p. 414–477.

Loucks, R.R., Premo, W.R., and Snyder, G.L., 1988. Petrology, structure, and age of the Mullen Creek layered mafic complex and age of accretion, Medicine Bow Mountains, Wyoming. *Geological Society of America. Abstracts with Programs*, v. 20, no. A73.

Love, J.D., and Christiansen, A.C., comps., 1985. Geologic map of Wyoming. U.S. Geological Survey, 3 sheets, scale 1:500,000. (Re-released 2014, Wyoming State Geological Survey).

Love, J.D., Christiansen, A.C., and Ver Ploeg, A.J., 1993. Stratigraphic chart showing Phanerozoic nomenclature for the state of Wyoming. Geological Survey of Wyoming [Wyoming State Geological Survey] Map Series 41.

Laft, S.J., 1985. Generalized geologic map showing distribution and basal configuration of the Browns Park Formation and Bishop Conglomerate in northwestern Colorado, northeastern Utah, and southern Wyoming. U.S. Geological Survey Miscellaneous Field Studies Map MF-182-1, scale 1:250,000.

McCallum, M.E., 1964. Petrology and structure of the Precambrian and post-Mississippian rocks of the east-central Medicine Bow Mountains, Albany and Carbon counties, Wyoming. Laramie, University of Wyoming, Ph.D. dissertation, 164 p.

McCallum, M.E., and Houston, R.S., 1985. Geologic map of the Albany quadrangle, Albany County, Wyoming. (unpublished mineral files): Geological Survey of Wyoming [Wyoming State Geological Survey]. 16 p., 1 pl., scale 1:24,000.

McCallum, M.E., and Orback, C.J., 1968. The New Rambler copper-gold-platinum district, Albany and Carbon counties, Wyoming. Geological Survey of Wyoming [Wyoming State Geological Survey] Preliminary Report 8, 12 p., 1 pl., scale 1:24,000.

Montagne, John, 1991. Cenozoic history of the Saratoga Valley area, Wyoming and Colorado. *Contributions to Geology*, v. 29, no. 1, p. 13–70, 1 pl., scale approx. 1:163,510.

Premo, W.R., and Loucks, R.R., 2000. Age and Pb-Sr-Nd isotopic systematics of plutonic rocks from the Green Mountain magmatic arc, southeastern Wyoming—Isotopic characterization of a Paleoproterozoic island arc system. *Rocky Mountain Geology*, v. 35, no. 1, p. 51–70.

Premo, W.R., and Van Schmus, W.R., 1989. Zircon geochronology of Precambrian rocks in southeast Wyoming and northern Colorado, in Grantling, J.A., and Tewksbury, B.J., eds., *Proterozoic geology of the southern Rocky Mountains. Geological Society of America Special Paper* 235, p. 13–32.

Ramirez, Octavio, 1971. Petrology and structure of the Precambrian metagneiss sequence in the Savage Run Creek area, Carbon County, Wyoming. Fort Collins, Colorado State University, M.S. thesis, 117 p., 1 pl., scale 1:16,000.

Sutherland, W.M., and Hansel, W.D., 2005. Preliminary geologic map of the Keystone quadrangle, Albany and Carbon counties, Wyoming. Wyoming State Geological Survey Open File Report 05-6, 22 p., 1 pl., scale 1:24,000.

Swetnam, M.N., 1961. Geology of the Pelton Creek area, Albany and Carbon counties, Wyoming. Laramie, University of Wyoming, M.S. thesis, 78 p., 1 pl., scale 1:15,500.

Ver Ploeg, A.J., Larsen, M.C., and Taboga, K.G., 2016. Characterization of evaporitic salt features in the southern Laramie Basin, Wyoming. Wyoming State Geological Survey Report of Investigations 70, 34 p.

NOTICE TO USERS OF INFORMATION FROM THE WYOMING STATE GEOLOGICAL SURVEY

The Wyoming State Geological Survey (WSGS) encourages the fair use of its material. We request that credit be expressly given to the "Wyoming State Geological Survey" when citing information from this publication. Please contact the WSGS at 307-766-2286, ext. 224, or by email at wgsinfo@wyo.gov if you have questions about citing materials, preparing acknowledgments, or extensive use of this material. We appreciate your cooperation.

Individuals with disabilities who require an alternative form of this publication should contact the WSGS. For the TTY relay operator, call 800-877-9975.

For more information about the WSGS or to order publications and maps, go to www.wsgs.wyo.gov, call 307-766-2286, ext. 224, or email wgs-info@wyo.gov.

NOTICE FOR OPEN FILE REPORTS PUBLISHED BY THE WSGS

Open File Reports are preliminary and usually require additional fieldwork and/or compilation and analysis; they are meant to be a first release of information for public comment and review. The WSGS welcomes any comments, suggestions, and contributions from users of the information.

DISCLAIMERS

Users of this map are cautioned against using the data as scales different from those at which the map was compiled. Using these data at a larger scale will not provide greater accuracy and is a misuse of the data.

The Wyoming State Geological Survey (WSGS) and the State of Wyoming make no representation or warranty, expressed or implied, regarding the use, accuracy, or completeness of the data presented herein, or of a map printed from these data. The act of downloading, copying, or printing this information from the WSGS website does not constitute a warranty. The WSGS does not guarantee the digital data or any map printed from the data to be free of errors or inaccuracies.

The WSGS and the State of Wyoming disclaim any responsibility or liability for interpretations made from, or any decisions based on, the digital data or printed map. The WSGS and the State of Wyoming retain and do not waive sovereign immunity.

The use of reference to trademarks, trade names, or other product or company names in this publication is for descriptive or informational purposes only, and is not intended to imply agreements between the products or the State of Wyoming and software or hardware developers/vendors, or pursuant to licensing agreements between the WSGS or the State of Wyoming and software or hardware developers/vendors, and does not imply endorsement of those products by the WSGS or the State of Wyoming.